International Journal of Heat and Mass Transfer xxx (2011) xxx–xxx

Contents lists available at ScienceDirect

International Journal of Heat and Mass Transfer

journal homepage: www.elsevier.com/locate/ijhmt

Direct simulation of turbulent heat transfer in swept flow over a wire in a channel

R. Ranjan [a], C. Pantano [a,*], P. Fischer [b]

[a] Department of Mechanical Science and Engineering, University of Illinois at Urbana-Champaign, 1206 West Green Street, Urbana, IL 61801, United States
[b] Mathematics and Computer Science Division, Argonne National Laboratory, Argonne, IL 60439, United States

ARTICLE INFO

Article history:
Available online xxxx

Keywords:
Turbulent swept flow
Direct numerical simulation
Passive scalar
Nusselt number
Flow over a wire
Channel flow

ABSTRACT

We investigate heat transfer characteristics of a turbulent swept flow in a channel with a wire placed over one of its walls using direct numerical simulation. This geometry is a model of the flow through the wire-wrapped fuel pins, the heat exchanger, typical of many civil nuclear reactor designs. The swept flow configuration generates a recirculation bubble with net mean axial flow. A constant inward heat flux from the walls of the channel is applied. A key aspect of this flow is the presence of a high temperature region at the contact line between the wire and the channel wall, due to thermal confinement (stagnation). We analyze the variation of the temperature in the recirculation bubble at Reynolds number based on the bulk velocity along the wire-axis direction and the channel half height of 5400. Four cases are simulated with different flowrates transverse to the wire-axis direction. This configuration is topologically similar to backward-facing steps or slots with swept flow, except that the dominant flow is along the obstacle axis in the present study and the crossflow is smaller than the axial flow, i.e., the sweep angle is large. The temperature field is simulated at three different Prandtl numbers: 10^{-2}, 10^{-1} and 1. The lower value of Prandtl number is characteristic of experimental high-temperature reactors that use a molten salt as coolant while the high value is typical of gas (or water vapor) heat exchangers. In addition, mean temperature, turbulence statistics, instantaneous wall temperature distribution and Nusselt number variation are investigated. The peak Nusselt number occurs close to the reattachment location, on the lee side of the wire, and is about 50–60% higher compared to the case without crossflow. The high temperature region follows the growth of the recirculation bubble which increases by about 65% from the lowest to highest amount of crossflow. Particular attention is devoted to the temperature distribution on the walls of the channel and the surface of the wire. The behavior of the heat-flux across the mean dividing streamline of the recirculation bubble is investigated to quantify the local heat transfer rates occurring in this region.

1. Introduction

Turbulent flows over complex geometries are routinely used to enhance mass and heat transfer, as well as mixing, in many industrial and chemical processes. Heat transfer enhancement caused by flow separation and reattachment, the type considered in the present study, has been studied extensively in many geometries [1]. Flow over a backward-facing step, forward-facing step, surface mounted rib, blunt flat plate and separated turbulent boundary layer are the most studied configurations in the literature. The behavior of the thermal boundary layer differs significantly between attached and separated flows [2]. Vogel and Eaton [3] studied heat transfer characteristics of the flow over a backward-facing step and found that a drop in the heat transfer coefficient occurs near flow separation and a rise occurs upstream of the flow reattachment zone. This particular variation of the heat transfer coefficient in this flow has been reported in several other studies [4–20]. Some other features of this configuration include correlation of turbulence intensity with the heat transfer coefficient near reattachment, recovery of Stanton number profile after reattachment towards equilibrium turbulent boundary layer value, correlation of r.m.s. of skin friction with the Stanton number and a persistent large disturbance in the outer part of thermal boundary layer after reattachment. Nassab et al. [21] studied heat transfer in flow over an inclined forward-facing step and reported that the Nusselt number reaches a maximum value near the reattachment location and decreases in the downstream direction after reattachment. Augmentation of heat transfer rate in flow over a blunt flat plate has been investigated in earlier studies [4,22–25] and it was found that vertical stirring of the flow caused by the vortical structures strongly enhance heat transfer. Similar to the flow over a backward-facing step, the heat transfer coefficient increases upstream of the reattachment zone. Placing a rib on a smooth surface to augment heat transfer has also been reported in numerous

* Corresponding author. Tel.: +1 217 244 1412; fax: +1 217 244 6534.
E-mail addresses: rranjan2@illinois.edu (R. Ranjan), cpantano@illinois.edu (C. Pantano), fischer@mcs.anl.gov (P. Fischer).

0017-9310/$ - see front matter © 2011 Published by Elsevier Ltd.
doi:10.1016/j.ijheatmasstransfer.2011.06.013

studies [17,26–32]. It has been found that the surface-averaged Nusselt number at the wall with the ribs, becomes large compared to that at the smooth wall. Rivir et al. [33] and Spalart and Strelets [34] studied the mechanism of heat transfer in a separated bubble and reported that the Reynolds analogy between wall heat transfer and momentum transfer in the separated region does not hold. In this region, the heat transfer coefficient is suppressed below the values observed in the attached region while it is much larger near reattachment when compared with the values in the attached boundary layer zone. A channel with an undulating wall or a two-dimensional hill has also been used for heat transfer enhancement and for studying complex convective and diffusive processes associated with the thermal field [35–37]. In this case, the average Nusselt number increases due to increased intensity and elongation of the near-wall streamwise vortices, which causes larger turbulence production and thus favors convection transport.

Far less is understood about temperature extrema in confined turbulent flows, both instantaneously and on the mean. This state of affairs arises because local extrema can only be investigated accurately using direct numerical simulation (DNS), which are not commonly employed in flows around complex geometries, due to the high computational cost. In simulations of these flows, the Reynolds averaged Navier–Stokes (RANS) approach is often employed [38,39]; for example in flow around a heat exchange assembly [40–42]. Nevertheless, even finely tuned turbulence models can only predict accurately mean and some times r.m.s. levels but not localized features of the profiles [43].

The flow configuration considered in this study is a simplification of the more complex arrangement encountered in a wire-wrapped nuclear fuel pin heat exchanger shown in Fig. 1, depicting results from a large-eddy simulation (LES) [44]. The mean flow goes from the bottom left corner to the upper right corner of the figure, in the direction along the fuel pins (large cylinders). A thin wire is stretched helically along the fuel pins to provide with a mechanism to maintain a turbulent flow and therefore ensure as high heat transfer rates as possible. The wrapped wires around the fuel pins can be seen clearly in Fig. 1, in the right-top corner of the fuel pins assembly. The flow over real wire-wrapped assemblies, which usually consists of hundreds of nuclear fuel pins with associated wires wrapped helically around them, is too complex to be accessible using DNS. Instead, the configuration studied here corresponds to an average situation in the real assembly. The simplified geometry is shown in Fig. 2 (further details will be provided below) and corresponds to the flow in a channel with a wire over one of its walls. Since the radius of curvature of the fuel pin is much larger than that of the thin wire, the local flow can be approximated to the flow over a flat surface with a wire resting on one of the surfaces. In this average situation, the bottom wall shown in Fig. 2 corresponds to the surface of the fuel pin on which the wire is wrapped and the top wall corresponds to the surface of the fuel pin above the wire on the opposite side. This simplified configuration is topologically similar to the class of swept backward facing step flows. Up-to-date, the only detailed simulations of these flows that have been performed at large sweep angles, which could be considered on their own right also as turbulent crossflow, are reported in [45]. Heat transfer in such cross-flow scenarios has not been exhaustively investigated in the past using DNS, although it represents a first order geometrical simplification of turbulent flows along complex wire-wrapped assemblies utilized in many civil nuclear reactors (the application that motivated this study). One noticeable difference between these flows and other backward facing step flows is that the flow within the recirculation region behind the wire is always fully turbulent, owing to the presence of a large axial flow. Note that the flow results reported in [45] and results for the heat-transfer reported in this study are based on same set of simulations, here temperature is considered as a passive scalar field.

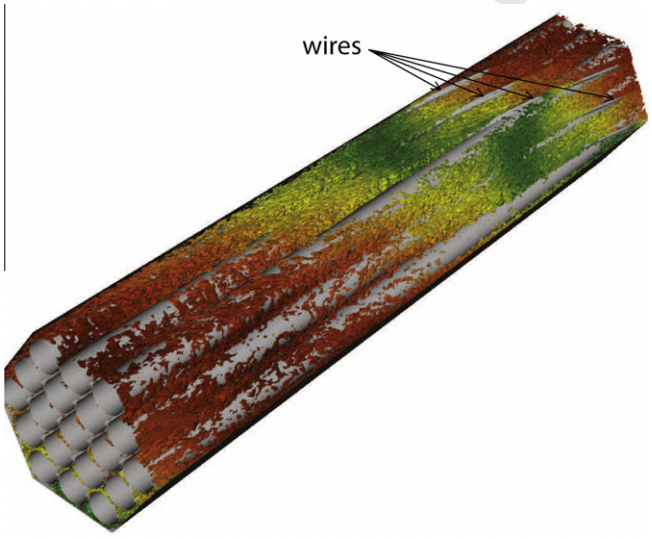

Fig. 1. Visualization of flow around a wire-wrapped nuclear fuel pin bundle at one instant from a simulation [44]. The contours are isosurfaces of velocity magnitude $U = \langle U \rangle$, the range of U is 0–2.68 $\langle U \rangle$ (peak), over 19 fuel pins. Pressure is plotted on the isosurfaces.

The mean temperature of the coolant will increase in the downstream direction when a constant heat flux is applied through the fuel pin surface in the wire-wrapped bundle. This will happen until the flow exits the heat exchanger, at which point the temperature will start to homogenize to a constant (high) value since no additional heat flux is introduced. Understanding the evolution of the temperature field in this 'spatial' configuration requires very large domains (in wire diameter units) and extreme resolution requirements at the Reynolds numbers of interest. Therefore, we have transformed the problem into a 'periodic' cell arrangement by extracting all the heat flux introduced at the walls by a volumetric sink (and therefore forcing the temperature field to remain periodic in the computational domain). We show that this configuration corresponds to the 'spatial' arrangement in an asymptotic limit, after a suitable transformation (described below). The objective of the present study is to perform a set of first principle DNS of moderately high Reynolds number in the relevant complex geometry and analyze the results to understand the nature of the mean temperature field, turbulence statistics, the variation of the Nusselt number, the distribution of instantaneous and mean wall temperature around the region of recirculation and to derive estimates of peak temperature as a function of Reynolds and Prandtl numbers. Heat transfer is investigated as the bulk crossflow velocity varies between 0% and approximately 32%, of the bulk axial velocity; or between 72° and 90° in terms of the sweep angle. Three different Prandtl numbers and four cross-flow rates are investigated. The Prandtl number is considered as low as 10^{-2} to include the regime encountered in experimental high-temperature reactors where the coolant is typically a molten salt, e.g., liquid lithium. The temperature field is assumed to be a passive scalar, since buoyancy effects are expected to be small at the scales of interest here. Finally, in addition to the results analyzed below, the databases can be used for comparisons and validation of LES and RANS models, e.g., [46–49].

2. Problem description

The problem considered in this study corresponds to a channel with a wire placed on the bottom wall of the channel. A schematic

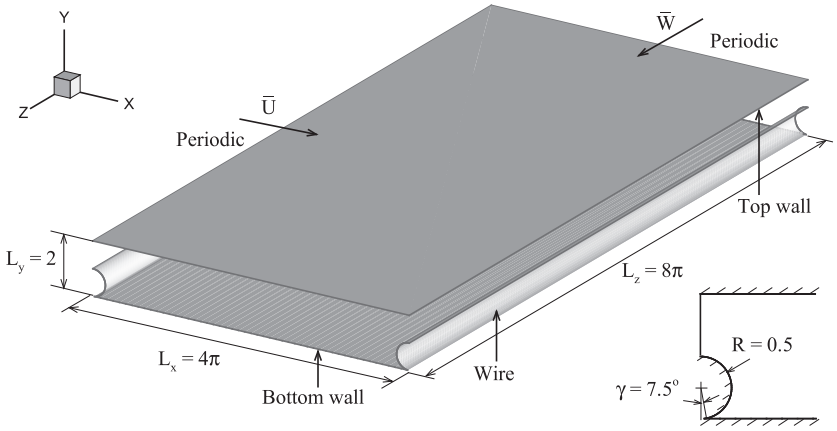

Fig. 2. Schematic of the geometry considered in the present study.

of the problem is shown in Fig. 2. The domain size is $L_x \times L_y \times L_z = 4\pi h \times 2h \times 8\pi h$ in the x, y and z directions, respectively. The x coordinate denotes the cross-flow direction, y is the vertical direction and z is the streamwise or axial direction. The cross-flow and axial directions are considered to be periodic. For convenience, the center of the cylindrical wire of radius $R = 0.5h$ is placed at the boundary of the periodic domain. Detailed justifications and resolution requirements for this flow, as well as turbulence statistics, are reported in Ranjan et al. [45].

In practical wire-wrapped assemblies, the wire is wrapped under tension around a nuclear fuel pin and there is a slight deformation of the wire at the contact location. To approximately model this detail we have chosen a finite contact angle between the wire and the wall of $2\gamma = 15°$, see right-bottom inset in Fig. 2. The flow in the channel is driven by the pressure gradient resulting from the imposed constant flowrates along the axial and cross-flow directions. In this study, the flowrate specified in the axial direction is higher than that imposed in the cross-flow direction. The resulting crossflow over the wire produces a large recirculation region or bubble with mean axial flow, in the lee side of the wire.

The boundary conditions for temperature consist of a constant and equal heat flux, q_w, at both walls of the channel and an adiabatic condition at the wire surface. These conditions approximate the situation encountered in the reactor passages. Presently, the channel walls would approximate the nuclear fuel pin surface, with a radius of curvature much larger than that of the wrapped wire, that radiates an approximately constant heat flux towards the cooling fluid. The wire is made of a non-nuclearly active material and therefore, to first approximation, there is no heat flux towards the channel. In reality, the wire thermal inertia may also play a role since some neutron radiation from the fuel pins affects the thermal behavior of the wire and heat transfer from the fluid and vice versa. These high-order effects are presently neglected because the heat transfer of nuclear origin from the fuel pins is usually large and the surface of the wire is much smaller than that of the fuel pin (the channel walls in the present case). The constant heat flux boundary condition is the limit of the conjugate heat transfer problem when the thermal activity approaches infinity [50,51]. In practice, the thermal activity is not extremely large for flow of molten coolant over a nuclear fuel pin surface. Hence, the equal flux boundary condition used in this study is an approximation of the real problem. The important aspect of this flow is that the presence of a recirculating zone enables the formation of a high-temperature region in the vicinity of the wire-wall contact line.

The presence of crossflow leads to the formation of a primary recirculation bubble in the lee side of the wire and two additional secondary bubbles in the lee and wind sides of the wire. Fig. 3(a) shows contours of the mean crossflow velocity normalized by bulk axial velocity and a projection of the mean streamlines in the $x - y$ plane for case C (see below). The primary and secondary bubbles are clearly evident close to the wire. After the flow detaches from the top surface of the wire, forming the shear layer over the primary bubble, it reattaches some distance downwind over the channel wall. After the flow reattaches, it starts to recover to equilibrium boundary layer flow, till it reaches the wind side of the wire where the flow separates again. The primary bubble is not closed in the mean sense, and it is in a fully turbulent state compared to a near laminar state of the separated region in canonical separating/reattaching flows. This is a consequence of the dominant turbulent axial flow. The flow to the center of the channel is similar to the flow in a canonical turbulent channel without obstructions. The effect of the wire is felt up to approximately two wire diameters, measured from the side boundaries. This causes a reduction in the vertical velocity gradient in those regions.

Fig. 3(b) and (c) show instantaneous vortical structures obtained using the λ_2-vortex criterion of [52], in the near-wall and recirculating regions in the cases without and with crossflow, respectively. Without crossflow, in the near-wall regions, elongated quasi-streamwise vortices are observed. In the shear layer region, intense vortical structures are observed with no preferential orientation. Near the reattachment region, the worm-like vortices get distorted because of the mean flow straining [53]. This is followed by recovery to boundary layer behavior, with vortical structures oriented along the quasi-streamwise direction [54,55].

A three-dimensional rendering of selected mean flow streamlines for a crossflow case near the wire is shown in Fig. 4. The spiral nature of the streamlines inside the separated bubble is apparent, showing the interaction of the crossflow with the axial flow. The streamlines emanating from above the bubble, s_1 and s_2, skip the bubble region. The streamlines within the bubble region; namely s_3, s_4, s_5 and s_6; show the mean rotational character of the flow. In the attached zone, the spiral nature is not observed as the velocity vector in the $x - y$ plane does not reverse direction. This type of spiral or helical path within the recirculating region is a characteristic of swept flows [56,57].

3. Mathematical formulation, approach and parameters

The motion of an incompressible fluid with constant density, ρ, and viscosity, μ, governed by the Navier–Stokes equations, is solved together with the continuity equation in the computational domain Ω. Periodic boundary conditions are employed along the axial and cross-flow directions and the no-slip boundary condition

Please cite this article in press as: R. Ranjan et al., Direct simulation of turbulent heat transfer in swept flow over a wire in a channel, Int. J. Heat Mass Transfer (2011), doi:10.1016/j.ijheatmasstransfer.2011.06.013

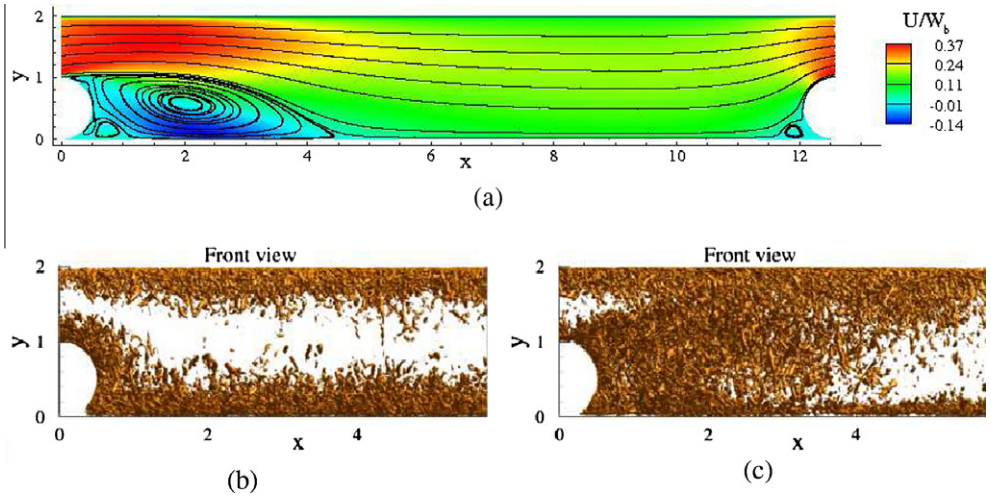

Fig. 3. Iso-contours of mean crossflow velocity normalized by bulk axial velocity and two-dimensional projection of the mean streamlines for case C (a) and instantaneous vortical structures in the near-wall and recirculation regions without, case A, (b) and with, case C, (c) crossflow.

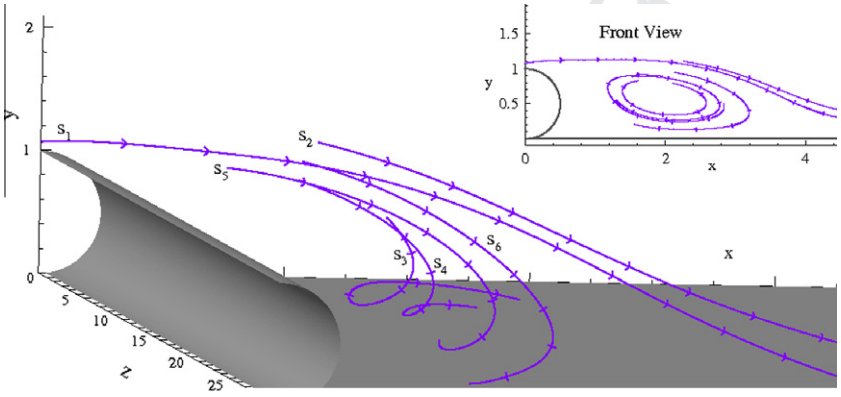

Fig. 4. Three-dimensional rendering of selected mean streamlines for case C with crossflow [45].

is used at the walls and at the surface of the wire. The mean flow, with axial and cross-flow components, is maintained by a constant pressure-gradient forcing imposed along these directions [45].

The velocity and temperature fields are advanced in time simultaneously, according to their governing equations for momentum and energy conservation. The equations are solved using a spectral element method implemented in *Prism* [58]. The equations are discretized using two-dimensional spectral elements in the $x-y$ plane and Fourier modes in the axial direction. Henderson and Karniadakis [59] provides more details of the method and the solution strategy.

All statistical quantities in the flow depend on the x and y coordinates. These ensemble mean quantities, denoted by $\langle . \rangle$, are obtained by averaging in time and in the simulations, where the flow is also homogeneous in the axial direction, means are obtained by averaging in the z direction as well. These running averages are determined only after the simulations reach a statistically steady state, as discussed in [45]. The flowrates are defined in the customary manner, according to:

$$Q_z = \int\int_{\Sigma} W(x,y)dxdy, \tag{1}$$

where Σ denotes the $x-y$ cross section of the domain and

$$Q_x = L_z \int U(x,y)dy, \tag{2}$$

with $\langle u \rangle = U$ and $\langle w \rangle = W$ denoting the average cross-flow and streamwise velocity component, respectively. The flowrates are not a function of z because the flow is homogeneous in this direction. The mean pressure-gradient forcing along the axial and cross-flow directions is denoted by $\bar{p}_z$ and $\bar{p}_x$, respectively. The flow is characterized by the bulk axial velocity, $W_b = Q_z/S(\Sigma)$, where $S(\Sigma)$ denotes the area of the $x-y$ cross-section of the domain, and the channel half height, h, as the characteristic velocity and length scales, respectively. These characteristic scales define the Reynolds number in the axial direction, given by

$$Re_z = \frac{\rho W_b h}{\mu}, \tag{3}$$

and the Reynolds number in the cross-flow direction, defined by

$$Re_x = \frac{\rho U_b h}{\mu}, \tag{4}$$

where $U_b = Q_x/(2hL_z)$ is the bulk velocity in the cross-flow direction, ρ denotes density and μ denotes dynamic viscosity. The overall Reynolds number is defined as:

$$Re_b = \sqrt{Re_x^2 + Re_z^2}, \tag{5}$$

and the local friction Reynolds number is given by

$$Re_\tau = \frac{\rho u_\tau h}{\mu}, \tag{6}$$

where u_τ denotes the average, in the statistically homogeneous directions, friction velocity, c.f., [45]. Note that Re_τ is a function of

Please cite this article in press as: R. Ranjan et al., Direct simulation of turbulent heat transfer in swept flow over a wire in a channel, Int. J. Heat Mass Transfer (2011), doi:10.1016/j.ijheatmasstransfer.2011.06.013

position along the walls of the channel and wire in the $x-y$ plane (quantities are averaged in z).

In the present problem, mean flow occurs in both axial as well as cross-flow directions and it is similar to three-dimensional turbulent boundary layers with cross-flow inhomogeneity. The Appendix describes the relationship between 'spatial' and 'periodic' arrangements of the temperature field and justifies the usage of periodic boundary condition in the present study through an asymptotic analysis. The dimensional, T, and non-dimensional, ϕ, temperatures are related by

$$T - T_b = \frac{q_w L}{\kappa}\phi, \tag{7}$$

where T_b is the average bulk temperature and $L = L_z$ denotes the axial length of the heat exchanger over which q_w acts. We can absorb T_b into T since the temperature obeys a linear partial differential equation. The Prandtl number is defined as $Pr = \mu C_p/\kappa$, where C_p denotes the specific heat capacity and κ denotes the thermal conductivity of the fluid. The relevant temperature statistical quantity is the local non-dimensional Nusselt number, Nu, given by

$$Nu = \frac{1}{\phi_w}, \tag{8}$$

where ϕ_w denotes the average value of ϕ at the wall. A wall temperature heat-flux based scale, ϕ_τ, akin to the friction velocity defined for velocity, is given by

$$\phi_\tau = \frac{1}{Re_\tau Pr}, \tag{9}$$

where Re_τ is the local friction Reynolds number at a particular location of the wall. The non-dimensional wall temperature heat-flux scale can be used to define an inner-scaled non-dimensional temperature, ϕ^+, given by

$$\phi^+ = \frac{\phi_w - \langle\phi\rangle}{\phi_\tau}. \tag{10}$$

Four simulations, labeled A through D, are investigated in this study with identical flowrate in the axial direction and varying flowrates in the cross-flow direction. In each of these cases the passive temperature field is simulated at two Prandtl numbers: 10^{-2} and 1. One additional simulation was carried out at Prandtl number of 10^{-1} for case C, totaling 9 simulations. The first case, A, has no crossflow over the wire and is considered as a reference scenario to compare with the other cases with crossflow, where recirculation bubbles are present. The crossflowrate increases, from cases B to D, to investigate the effect of the wire and overall flow and heat transfer behavior. Table 1 lists some of the parameters of these simulations, including all the Reynolds numbers defined above and the normalized mean pressure-gradient forcing along the axial and cross-flow directions. The low value of Prandtl number, i.e., $Pr = 10^{-2}$, is considered to include the regime encountered in experimental high-temperature reactors where typically a liquid coolant is used. The flow field is initialized as described in [45] and turbulence statistics were gathered after the initial transients had subsided. These simulations were carried out using a mesh containing a total of 936 macro elements in the $x-y$ plane. Each of these elements are further resolved by a 15^{th} order polynomial. A total of 512 Fourier modes are used in the homogeneous z direction, resulting in an overall 107, 827, 200 collocation points. Further details of the initialization and grid choice are described in [45], including the adequacy of the grid spacing at the present Reynolds numbers. Moreover, this grid is sufficient for the study of the heat transfer problem discussed here since the Prandtl numbers are less or equal to one. The temperature lengthscales are equal or larger than the Kolmogorov scale [60].

Table 1
Simulation parameters for all cases.

Case	Re_z	Re_x	Re_b	$\langle Re_\tau\rangle$	Q_z	Q_x	$2h\bar{p}_z/\rho W_b^2$	$2h\bar{p}_x/\rho W_b^2$
A	5400	0	5400	305	21.94	0	7.7×10^{-3}	0
B	5400	417	5416	307	21.94	3.49	7.9×10^{-3}	1.5×10^{-3}
C	5400	842	5465	312	21.94	7.05	8×10^{-3}	4.6×10^{-3}
D	5400	1709	5664	335	21.94	14.32	9×10^{-3}	1.6×10^{-2}

4. Surface temperature distribution

The temperature distribution on the walls of the channel and wire surface, in particular the peak values can play an important role in the material integrity of the heat exchanger. These quantities are investigated in this section. The instantaneous surface temperature distribution is studied qualitatively to investigate the effect of crossflow and Prandtl number.

4.1. Instantaneous fields

Iso-contours of ϕ on the bottom wall including the wire surface at $Pr = 1$ are shown in Fig. 5. In general, the temperature is higher in the vicinity of the contact line between the wire and the channel wall. This is due to flow confinement which restricts outward heat transport. The mechanism of heat transfer is therefore dominated by thermal conduction, since advection is not effective in the corner regions of the wire. The extent of this high-temperature region increases in the x direction with increasing crossflow; increase in the extent of the primary separated region. Moreover, with all other parameters fixed, the high-temperature region should diminish with increasing Reynolds number, as higher intensity turbulent fluctuations are able to penetrate deeper in the wall layer. Towards the center of the channel, the surface temperature adopts a regular and classical distribution similar to that observed in turbulent flows with heat transfer [61–63]. This includes a qualitatively streaky pattern, with regions of higher value of temperature embedded in low value regions, aligned in the mean with the flow direction. In case A, the regions of low and high temperature streaks appear elongated in the axial direction with spacing in the crossflow direction. As mentioned in several studies [61,64,65], the temperature field in the near-wall regions correlates well with the streamwise velocity. In particular, high temperature is correlated with high speed fluid and vice versa. In the cases with crossflow, away from the wire, the streaky structures are elongated along the net mean flow direction which is inclined along the axial direction. Such streaky structures in the temperature field are also observed downstream of the reattachment in other separating/reattaching flows [13,16,66]. In the lee-ward side of the wire, under the primary recirculation bubble, the streaky structures are not as marked as those observed towards the center of the channel. This can be attributed to the thermal confinement effect mentioned earlier which leads to a relatively lower level of temperature fluctuations in this region. This is in contrast with the wind-ward side of the wire, where the streaky pattern of ϕ is still observed. Compared to canonical separating/reattaching flows, the temperature field in the present simulations still shows a streaky pattern under the recirculating bubble. In the canonical cases, the temperature distribution is smeared due to laminarization, however in the present flow configuration this is not the case due to presence of a turbulent axial flow. This is a major difference with canonical backward-facing step.

Surface temperature isocontours at the bottom wall and on the wire for $Pr = 10^{-2}$ are shown in Fig. 6 for all cases. At this low Prandtl number, and moderate Reynolds number, one does not ob-

Please cite this article in press as: R. Ranjan et al., Direct simulation of turbulent heat transfer in swept flow over a wire in a channel, Int. J. Heat Mass Transfer (2011), doi:10.1016/j.ijheatmasstransfer.2011.06.013

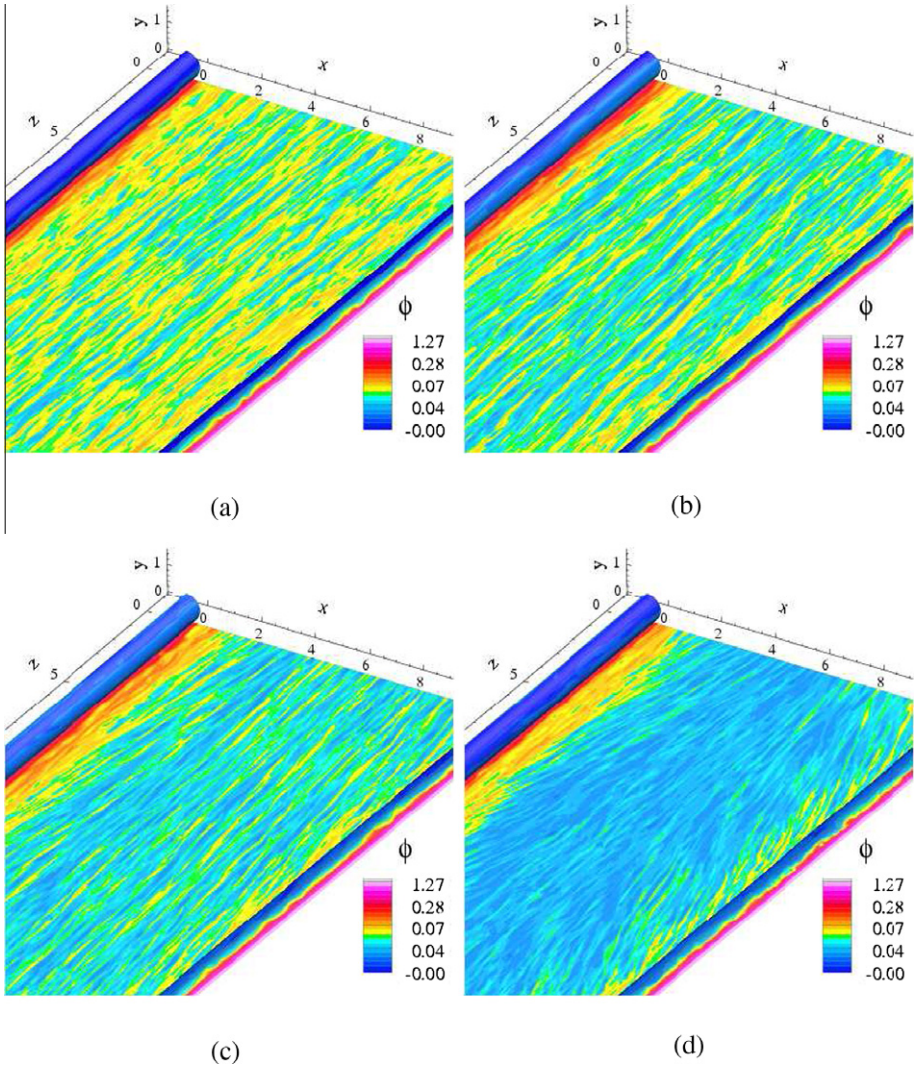

Fig. 5. Iso-contours of ϕ at $Pr = 1$, on the bottom wall including the wire surface. Subfigures denote cases A (a), B (b), C (c) and D (d).

serve a wall-layer with a streaky structure as the smallest scale of temperature fluctuation increases with decreasing Prandtl number [60,67,68]. This is apparent in case A where a spot-like pattern is observed in the central part of the channel. The spot-like pattern shows regions of higher temperature values lying between large regions of smaller temperature values. As before, one still observes relatively high temperature around the wire contact line, which are confined around the recirculation regions. When recirculation is present, no preferential alignment of the spots along the net mean flow direction is observed. Note also that the extent of the high-temperature region in the lee-ward side of the wire remains approximately of the same size while it decreases in size in the wind-ward side with increasing crossflow. For completeness, one simulation was carried out at $Pr = 10^{-1}$ with the conditions of case C, shown in Fig. 7. In this case, the patterns resemble those observed in the cases at $Pr = 1$ discussed before. One notable difference is the disappearance of characteristic elongated structures in the recirculation zones where the temperature is high. The surface distribution of ϕ for this Prandtl number indicates a transition from the spot-like pattern observed at $Pr = 10^{-2}$ to the streaky pattern observed for $Pr = 1$. Overall, the distribution of ϕ on the bottom wall for the lower Prandtl number cases looks significantly different from that at the higher Prandtl numbers. This occurs because at lower Prandtl number, the thickness of the inner thermal layer is much larger than that of the velocity and the temperature field does not correlate very well with the streamwise velocity fluctuations near the wall [61,69].

4.2. Mean and root-mean-square wall temperature

The variation of $\langle\phi\rangle$ along the wire surface at the two Prandtl numbers is shown in Fig. 8, for all cases in polar coordinates. At $Pr = 1$, a sharp increase in $\langle\phi\rangle$ is observed towards the contact line of the wire with the channel wall. This sharp increase occurs because of thermal confinement. In this region, the mechanism of heat flux is dominated by thermal diffusion as discussed before, since advection is not as effective in the corner regions of the wire. The temperature increase is observed for all cases. However, the increase occurs gradually at the low Prandtl number cases and is not as sharp as that observed in the high Prandtl number cases. Away from the contact line of the wire with the channel wall, the profile of mean temperature remains nearly uniform at both Prandtl numbers. At $Pr = 1$, in case A, the mean temperature is slightly negative over the wire region for β approximately lying between 20° and 160°. However at $Pr = 10^{-2}$, the mean temperature is negative over the wire for β lying between 30° and 150° in all the cases. The positive temperature over the wire surface in the cases with cross-flow at $Pr = 1$ can be attributed to a relatively

Please cite this article in press as: R. Ranjan et al., Direct simulation of turbulent heat transfer in swept flow over a wire in a channel, Int. J. Heat Mass Transfer (2011), doi:10.1016/j.ijheatmasstransfer.2011.06.013

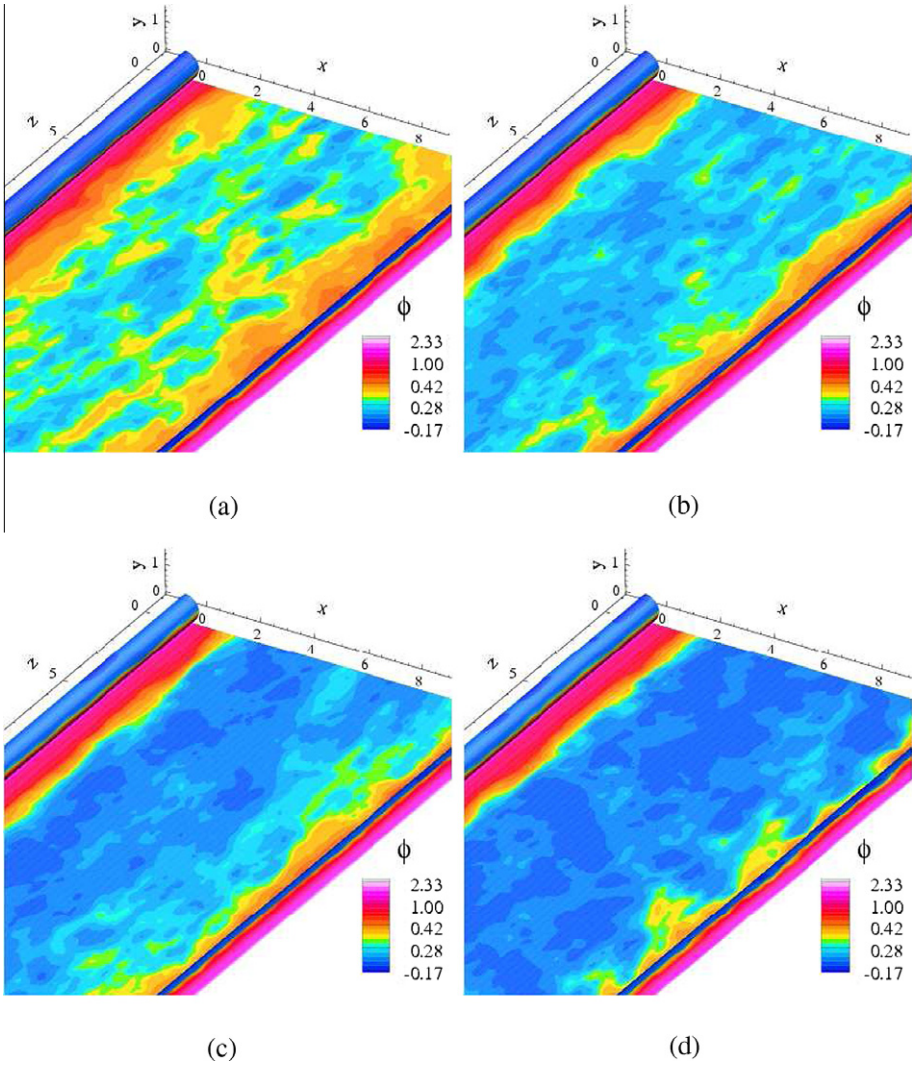

Fig. 6. Iso-contours of ϕ at $Pr = 10^{-2}$, on the bottom wall including the wire surface. Subfigures denote cases A (a), B (b), C (c) and D (d).

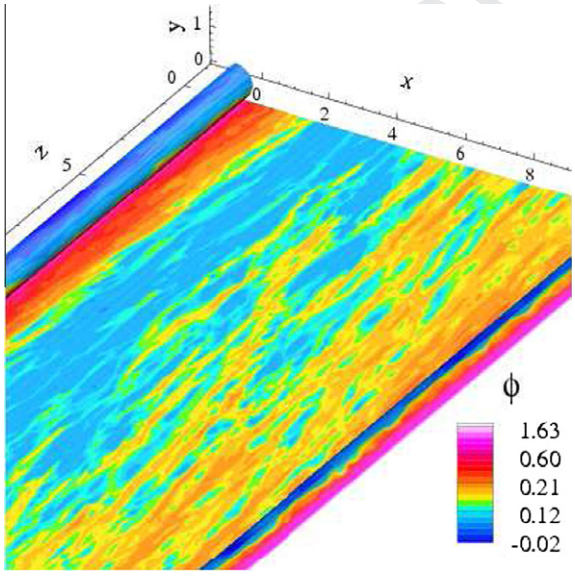

Fig. 7. Iso-contours of ϕ at $Pr = 10^{-1}$, on the bottom wall including the wire surface for case C.

higher level of mixing of the hotter fluid near the top wall with the colder fluid near top of the wire. The profiles appear insensitive to the level of crossflow (for the values considered in this study) but much more sensitive to the Prandtl number. The variation of $\langle\phi\rangle$ along the bottom wall of the channel is equivalent to the variation of *Nu*, since the Nusselt number is related to the mean temperature on the bottom wall through Eq. (8). The variation of *Nu* on the bottom wall is discussed in the next section.

The variation of the root-mean-square temperature value, denoted by ϕ_{rms}, along the crossflow direction on the bottom wall of the channel is shown in Fig. 9, for the two Prandtl numbers and all cases. High values of ϕ_{rms} are observed in the vicinity of the wire for $Pr = 1$ in all cases. Such increase in the level of temperature fluctuations is closely associated with an accelerating and decelerating flow in the vicinity of the wire which results in a larger level of velocity fluctuations. In the cases with crossflow, the peak value towards the wind-ward side of the wire is higher than that in the lee-ward side. This is because higher level of fluctuations are tied to an accelerating flow than a decelerating flow [70]. The difference between these peaks increases as crossflow increases. A sharp decrease in ϕ_{rms} is observed towards the center of the channel; which is approximately constant in case A. In the cases with crossflow, a local peak is observed under the separated flow region. These local peaks broadens with increasing crossflow.

Please cite this article in press as: R. Ranjan et al., Direct simulation of turbulent heat transfer in swept flow over a wire in a channel, Int. J. Heat Mass Transfer (2011), doi:10.1016/j.ijheatmasstransfer.2011.06.013

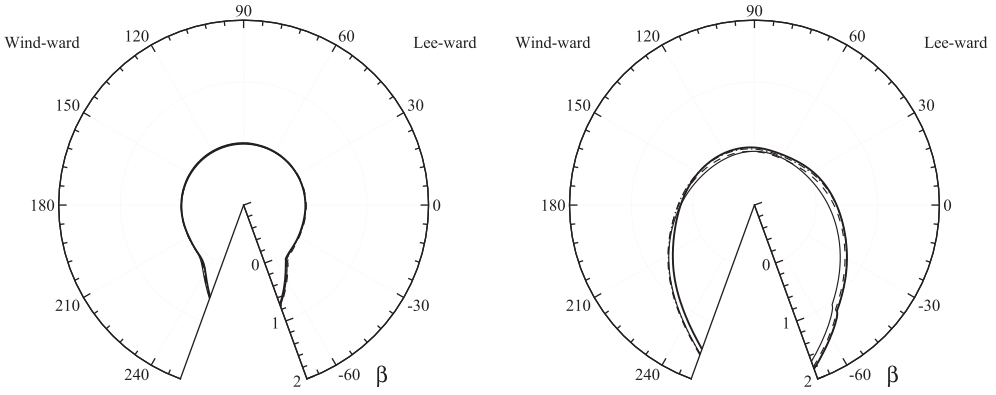

Fig. 8. Variation of $\langle\phi\rangle$ on the wire-surface. Cases A, B, C and D are denoted by thin solid, thin dashed, thin dashed-dotted and thick solid curves, respectively.

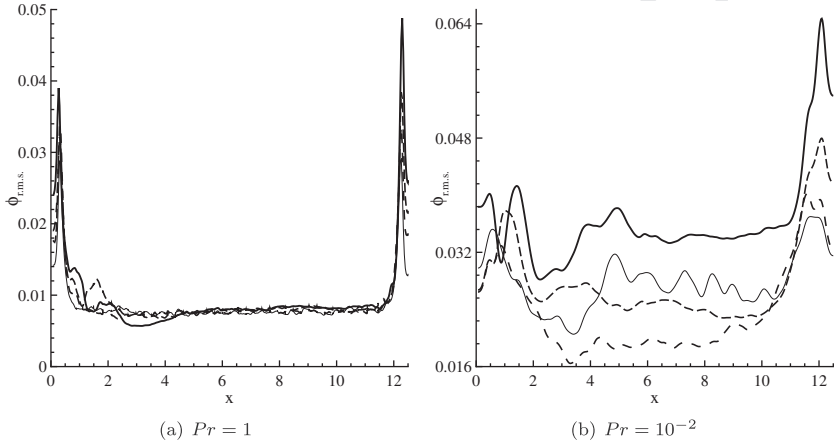

Fig. 9. Variation of ϕ_{rms} on the bottom wall of channel. Cases A, B, C and D are denoted by thin solid, thin dashed, thin dashed-dotted and thick solid curves, respectively.

Their presence can be attributed to the growth of the secondary bubble in the lee-ward side of the wire and increased level of turbulence inside the recirculation bubble, which is in a turbulent state due to presence of the large axial flow. After this local peak, ϕ_{rms} decreases until it reaches a minimum before reattachment, with a gradual increase towards the center of the channel. The decrease near reattachment and subsequent increase to equilibrium levels indicates the recovery of the thermal boundary layer. The rate of increase is higher in the case with the highest crossflow. Towards the wind-ward side of the wire, a small decrease is observed before increasing sharply to a large value at the corner of the wire. At lower Prandtl number, a qualitatively similar behavior is observed in all the crossflow cases. Local peaks are observed in both the lee- and wind-ward sides of the wire with peak values on the wind-ward side higher than on the lee-ward side. The wind-ward side peak value increases with increasing crossflow. The overall magnitude of ϕ_{rms} increases, as expected, in the central part of the channel with increasing crossflow. Thus the variation of ϕ_{rms} is closely tied to the behavior of the flow, i.e., the magnitude of the temperature fluctuations is affected significantly by the separating/reattaching and recovering flow and increasing strength of the crossflow.

The variation of ϕ_{rms} along the wire surface for the two Prandtl numbers is shown in Fig. 10, for all cases in polar coordinates. In case A, a symmetric variation is observed at both Prandtl numbers. In the cases with crossflow, the value of ϕ_{rms} increases from a lower value at the wire top and it reaches a peak close to, but not at, the wire contact line at both Prandtl numbers. The variation of ϕ_{rms} on the wire has an asymmetrical shape with larger values on the wind-ward side of the wire. As mentioned earlier, the increased temperature fluctuation is tied to accelerating and decelerating flow on the lee-ward and wind-ward side of the wire. The temperature fluctuation increases over the wire surface with increasing crossflow, due to increased mixing by the turbulent flow. This increase is clearly evident at the lower Prandtl number. The variation of ϕ_{rms} is qualitatively similar to the variation of the r.m.s. of τ_w [45] on the wire surface which again implies that the temperature fluctuations are well correlated with the velocity fluctuations.

4.3. Peak mean temperature scaling

The maximum temperature occurs in the immediate vicinity of the wire contact line and it is important from a practical point of view; the design of the reactor subassembly mandates material integrity of the heat exchanger. The difference between the maximum instantaneous temperature and the maximum mean temperature is very small in these simulations. This is likely caused by the reduced level of turbulence fluctuations around the corner. The maximum value of the mean non-dimensional temperature, $\langle\phi\rangle_{max}$, occurs at the wire-wall contact point in the lee-ward side in all the simulations and it is a function of the Reynolds and Prandtl

Please cite this article in press as: R. Ranjan et al., Direct simulation of turbulent heat transfer in swept flow over a wire in a channel, Int. J. Heat Mass Transfer (2011), doi:10.1016/j.ijheatmasstransfer.2011.06.013

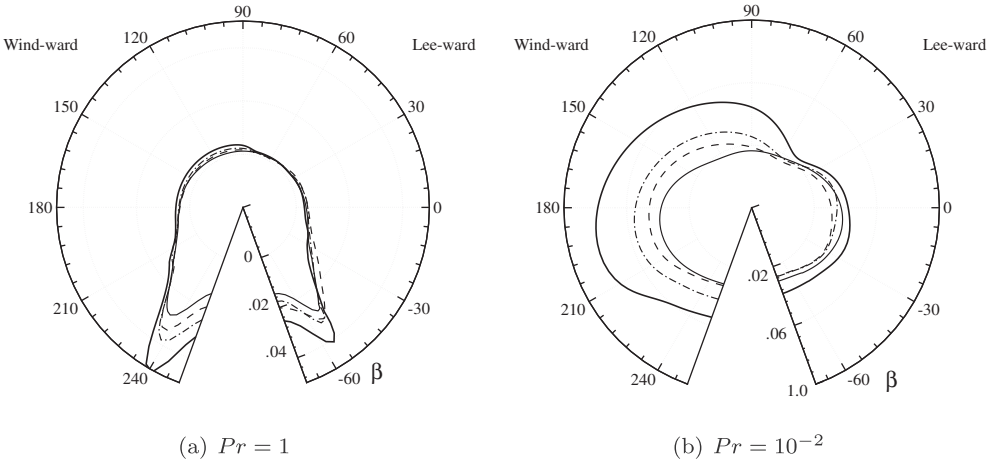

(a) $Pr = 1$ (b) $Pr = 10^{-2}$

Fig. 10. Variation of ϕ_{rms} on the wire-surface. Cases A, B, C and D are denoted by thin solid, thin dashed, thin dashed-dotted and thick solid curves, respectively.

numbers. Since the range of Reynolds numbers of these simulations is very narrow (for our range of sweep angles), we can not ascertain the dependence of the maximum temperature on Re_x. We observe primarily the effect of Prandtl number. A scaling is proposed to parametrize the maximum temperature, $\langle\phi\rangle_{max}$, in terms of the molecular Prandtl number, using the simulation data. This simple scaling relation is given by

$$\langle\phi\rangle_{max} = \mathscr{C} Pr^{\eta}, \tag{11}$$

where $\mathscr{C}$ is a function of Reynolds number and in our case it is approximately 1.22 while $\eta = -0.13$. The value of the constants $\mathscr{C}$ and η are obtained by performing a best fit to the simulation data at the three Prandtl numbers: 10^{-2}, 10^{-1} and 1. The variation of the maximum temperature, $\langle\phi\rangle_{max}$, with Prandtl number is shown in Fig. 11 on a log–log scale which also shows the scaling relation given by Eq. (11). It is observed that as Pr increases, $\langle\phi\rangle_{max}$ decreases linearly on the logarithmic scale. The relation given by Eq. (11) can be used to predict the value of maximum temperature at Prandtl numbers ranging from 10^{-2} to 1. Note that the scaling relation proposed here considers lower values of Prandtl number to include the regime encountered in experimental high-temperature reactors.

5. Temperature statistics

In this section, mean temperature profiles are investigated first, both in the original coordinates and in the inner-scaled coordinate

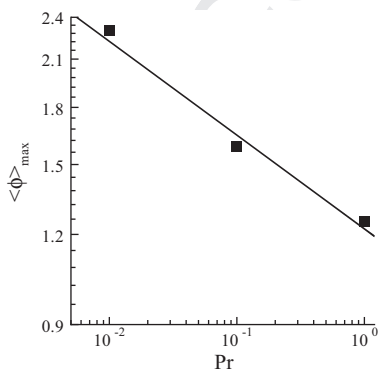

Fig. 11. Variation of maximum mean temperature, $\langle\phi\rangle_{max}$, with Prandtl number. Symbols indicate simulation data and the solid curve denotes the scaling relation given by Eq. (11).

frame. In addition, the behavior of the Nusselt number is discussed. All velocity statistics are discussed in [45]. This is followed by a discussion of the behavior of the temperature intensity and mean axial and vertical heat fluxes at particular planes across the flow. The detailed discussion of first- and second-order statistics of the temperature field in this section, illustrates the role of crossflow and Prandtl number for this turbulent swept flow configuration.

5.1. Mean temperature field and Nusselt number

Iso-contours of the mean non-dimensional temperature, $\langle\phi\rangle$, for $Pr = 1$ and 10^{-2} are shown in Figs. 12 and 13, respectively, for all cases. Case A in Fig. 12 shows symmetry about the mid-plane due to the symmetry of the geometry and boundary conditions. Even in this case, high temperature regions are observed in the corner region where the wire contacts the bottom wall of the channel. This is a consequence of the nearly stagnant flow, very low velocities, in these regions; advection of the temperature field by the flow field, out of this region is quite ineffective due to confinement. The effect of the wire is felt up to approximately two wire diameters measured from its center. In this region, there is a decrease in the temperature gradient in the wall-normal direction near the walls. Away from the wire and towards the center of the channel, the temperature contours are similar to those observed in earlier studies of passive scalars in a turbulent channel flow. In the cases with crossflow, a primary recirculation zone forms in the lee-ward side of the wire and two secondary recirculating zones form both on lee- and wind-ward side of the wire. The turbulence statistics of these separated-flow regions are discussed in detail in [45]. Similar to case A, regions of high temperature are observed in the corner of the wire with the wall and in the separated flow regions. In the primary recirculation region, there is less efficient distribution of heat flux coming from the wall with the rest of the flow in the channel and this results in a net rise in the temperature values in the bubble. This is similar to the temperature rise observed in the separated region in the flow over a backward-facing step [8,10] and in the lee-ward side of a two dimensional hill [37]. The size of the primary recirculation bubble grows with increasing crossflow and this leads to an increase in the size of the region having higher temperatures. The growth of the high temperature region follows the growth of the recirculation bubble in terms of the reattachment length, which increases by about 65% from the lowest to highest crossflow. Moreover, away from the recirculation zones, the thickness of the thermal boundary layer near the walls changes with increasing crossflow, in particular the bottom-wall thickness seems to decrease while the top-wall thickness seems

Please cite this article in press as: R. Ranjan et al., Direct simulation of turbulent heat transfer in swept flow over a wire in a channel, Int. J. Heat Mass Transfer (2011), doi:10.1016/j.ijheatmasstransfer.2011.06.013

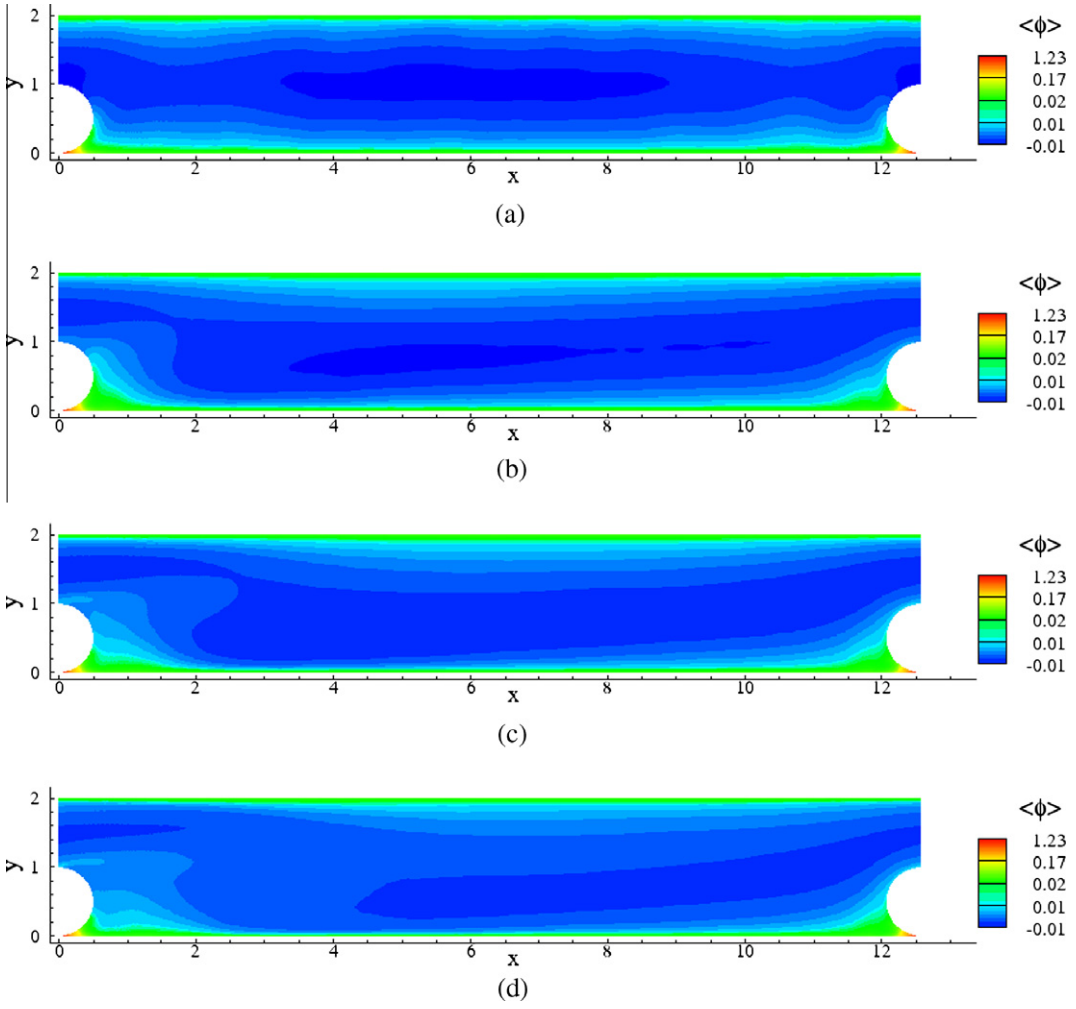

Fig. 12. Iso-contours of mean non-dimensional temperature, $\langle\phi\rangle$ at $Pr = 1$, for cases A (a), B (b), C (c) and D (d).

to increase. The results for $Pr = 10^{-2}$ are qualitatively similar except that the thickness of the thermal layer is much larger, as expected. One difference with the higher Pr case is that the mean temperature in the primary recirculation zone barely changes with increasing crossflow; thermal diffusion dominates over advection.

Mean temperature profiles scaled with the wall temperature flux, inner coordinates, along the wall normal direction, y, at different crossflow locations is investigated next. The profiles are extracted at the locations denoted by x_t, x_c, x_b and x_r, corresponding to the top of the wire, center of the channel, center of the primary recirculation zone and reattachment point, respectively. Only the locations x_t and x_c are considered for case A, since it has no recirculation zone. The crossflow locations for all simulations are summarized in Table 2. The profiles of the normalized temperature, ϕ^+, are shown in Figs. 14 and 15 as a function of the inner coordinate y^+ measured from the bottom and top walls, respectively. These profiles have been extracted at each of the locations indicated previously. The profiles measured from the bottom wall do not include the location x_t, as the wall temperature flux, ϕ_τ, is zero on the surface of the wire; adiabatic boundary condition. The values of the non-dimensional temperature flux, ϕ_τ, at the bottom and top walls at different crossflow locations are shown in Table 3 at two Prandtl numbers. Figs. 14 and 15 also show the recommended formula provided by Kader [71]. The suggested formula is a function of Prandtl number and Reynolds number and is based on a survey of several experimental results. The recommended formula has a logarithmic region away from the wall where the normalized mean temperature varies linearly with respect to y^+, on the logarithmic scale.

As indicated in [45], one does not expect that universal scaling laws will be applicable in the present flow over a complex boundary. This is a consequence of the moderately high Reynolds number and the anisotropies and inhomogeneities induced by the presence of the wire. Nevertheless, the reference or ideal profiles gives a baseline comparison with the present results. Fig. 14(a) and (b) show the inner-scaled temperature profiles at location x_c, center of the channel, from the bottom wall, at $Pr = 1$ and 10^{-2}. As expected, all the cases show a collapse with the recommended formula in the inner conductive sublayer region at both low and high Prandtl numbers. Case A approximately collapses to the recommended formula in the logarithmic region at $Pr = 1$. At the lower Prandtl number, only a conductive sublayer is observed for higher y^+ values and the profile shows a deviation for $y^+ \gtrsim 50$ from the ideal profile. The thickness of the inner conductive sublayer increases as Prandtl number decreases [68,72]. In all the cases with crossflow, deviation from the ideal profile is observed for $y^+ \gtrsim 30$ at both Prandtl numbers. Fig. 14(c) and (d) show profiles at location x_b for $Pr = 1$ and 10^{-2}, respectively. All the profiles at this location collapse with the recommended formula in the inner conductive sublayer region but not in the region away from the inner sublayer. The deviation in the latter region increases with crossflow. This feature is common at both Prandtl numbers. This

Please cite this article in press as: R. Ranjan et al., Direct simulation of turbulent heat transfer in swept flow over a wire in a channel, Int. J. Heat Mass Transfer (2011), doi:10.1016/j.ijheatmasstransfer.2011.06.013

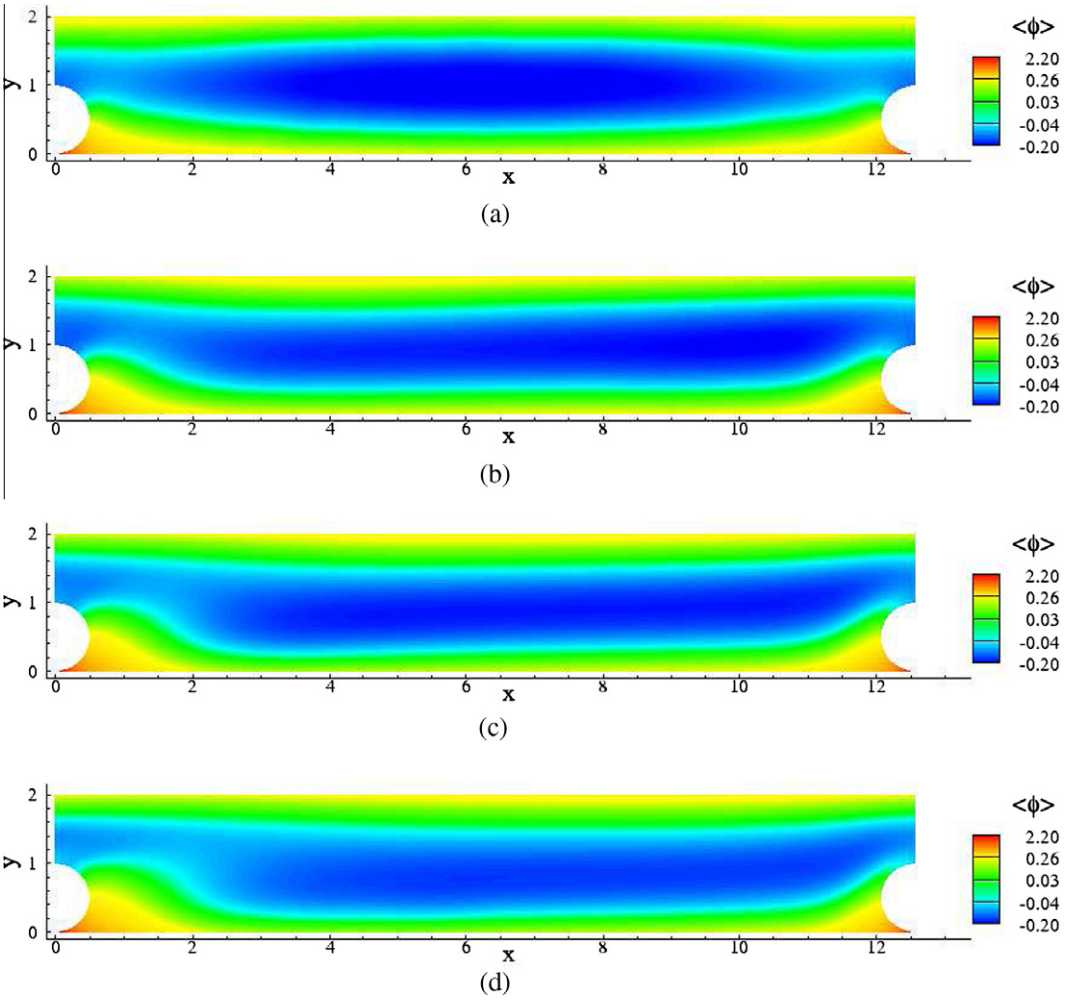

Fig. 13. Iso-contours of mean non-dimensional temperature, $\langle\phi\rangle$ at $Pr = 10^{-2}$, for cases A (a), B (b), C (c) and D (d).

Table 2
Particular locations of interest along the cross-flow direction.

Case	Spanwise locations			
	x_t/h	x_c/h	x_b/h	x_r/h
A	0	2π	–	–
B	0	2π	1.39	3.32
C	0	2π	2.01	4.67
D	0	2π	2.46	5.55

behavior is different from the study of heat transfer in flow over a backward-facing step, where even the thermal "Law of the Wall" is not followed under the separated region [8]. This difference can be attributed to a fully turbulent state of the recirculating bubble, which is a unique feature of the present flow. The profiles at location x_r, are shown in Fig. 14(e) and (f) for $Pr = 1$ and 10^{-2}, respectively. These profiles are similar to those at x_c.

Overall, as expected, the normalized temperature profiles agree reasonably well with the recommended formula in the inner conductive sublayer region. Outside the inner sublayer, deviations are observed which tend to be more pronounced with increasing crossflow. The value of ϕ^+ in this region is lower than the value predicted by the recommended formula. These deviations are observed at all the crossflow locations for the lower Prandtl number cases. The deviation at the reattachment location can be attributed to the strong non-equilibrium and anisotropy of the thermal boundary layer due to presence of large scale coherent structures impinging from the shear layer. This deviation persists at x_c in case D, given the slow recovery of the thermal boundary layer after reattachment.

Fig. 15(a) and (b) show the profiles of ϕ^+ at x_c, measured from the top wall for $Pr = 1$ and 10^{-2}, respectively. As expected, all the profiles collapse with the recommended formula in the inner conductive sublayer for both Prandtl numbers. The logarithmic region of the recommended formula is evident for $Pr = 1$ and all profiles agree well with the recommended formula. But this is no longer the case for the lower Prandtl number case where only the conductive sublayer is present, discrepancies are clearly observed. Fig. 15(c) and (d) show the profiles at x_t where the profiles with zero crossflow is close to the recommended formula but they start to depart as the crossflow increases. The deviation for $Pr = 1$ is mostly an increase in the value of the slope intercept in the logarithmic region, ϕ^+ increases with crossflow. Similar to the velocity profile [45], this deviation can be attributed to effect of curvature of wire. The profiles at location x_b, shown in Fig. 15(e) and (f), again collapse in the inner conductive sublayer region for both Prandtl numbers. In the logarithmic region, for $Pr = 1$, the value of ϕ^+ increases with increasing crossflow. However at $Pr = 10^{-2}$, ϕ^+ decreases with increasing crossflow in the outer part of the conductive sublayer. This causes a deviation from the recommended formula, which is more significant at lower Prandtl number. The profiles at location x_r, shown in Fig. 15(g) and (h), collapse

Please cite this article in press as: R. Ranjan et al., Direct simulation of turbulent heat transfer in swept flow over a wire in a channel, Int. J. Heat Mass Transfer (2011), doi:10.1016/j.ijheatmasstransfer.2011.06.013

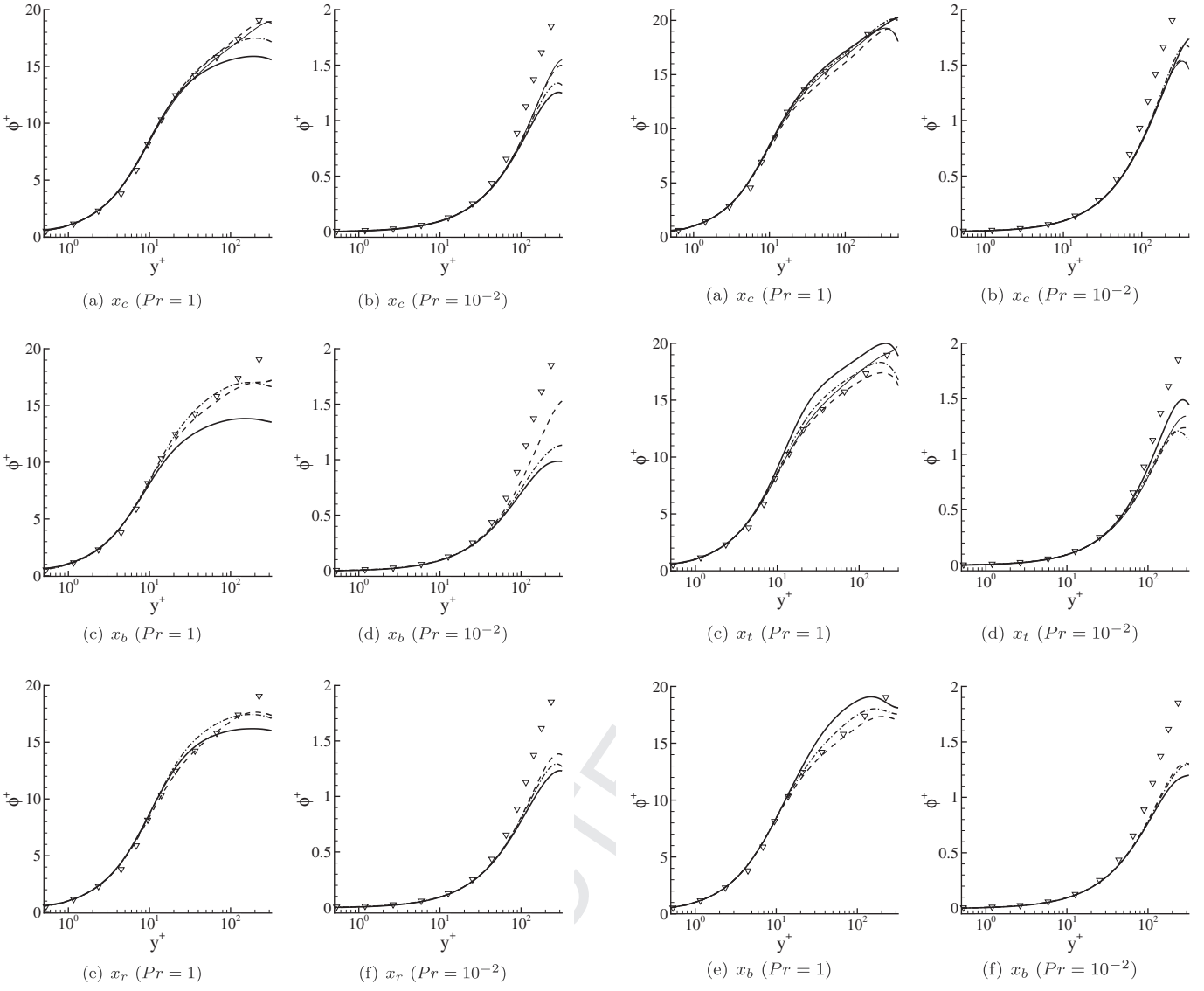

Fig. 14. Profiles of mean temperature normalized with the wall surface temperature flux at different cross-flow locations measured from the bottom wall. Cases A, B, C and D are denoted by thin solid, thin dashed, thin dashed-dotted and thick solid curves, respectively. Symbol (▽) denote the recommended formula provided by Kader [71].

Fig. 15. Profiles of mean temperature normalized with the wall surface temperature flux at different cross-flow locations measured from the top wall. Cases A, B, C and D are denoted by thin solid, thin dashed, thin dashed-dotted and thick solid curves, respectively. Symbol (▽) denote the recommended formula provided by Kader [71].

in the inner conductive sublayer, similar to that observed at other locations. At $Pr = 1$, cases B and C show reasonable collapse with the recommended formula in the logarithmic region, whereas case D has lower values of ϕ^+ in this region.This can be attributed to a larger cross-flow in case D which results into larger non-equilibrium effects at this location. At $Pr = 10^{-2}$, all the crossflow profiles collapse in the outer part of the conductive sublayer region, but deviate from the recommended formula.

In conclusion, the normalized mean temperature profiles agree well with the recommended formula of Kader [71] in the inner conductive sublayer region as well as the logarithmic region when the flow is attached and in particular for $Pr = 1$, which is expected. When the crossflow increases and detached regions form and for the low Prandtl number case, the deviation in the outer conductive sublayer region become apparent. The effect of crossflow is significant in the case with the largest crossflow due to increased level of fluctuations in the separated region which persists in the crossflow direction in the outer part of the thermal boundary layer leading to a slower recovery. Note that this recovery of thermal boundary layer is still faster in the present cases compared to the canonical separating/reattaching flows due to presence of a dominant turbulent axial flow.

The Nusselt number, *Nu*, represents the ratio of convective to conductive heat flux and is an useful physical quantity for the understanding of the effectiveness of the heat transfer process.

Please cite this article in press as: R. Ranjan et al., Direct simulation of turbulent heat transfer in swept flow over a wire in a channel, Int. J. Heat Mass Transfer (2011), doi:10.1016/j.ijheatmasstransfer.2011.06.013

Table 3
Non-dimensional temperature flux, ϕ_τ, at different cross-flow locations. Subscripts b and t denote values at bottom and top wall, respectively.

Case	Temperature flux $\times 10^3$	$Pr = 1$ Spanwise locations				$Pr = 10^{-2}$ Spanwise locations			
		x_t/h	x_c/h	x_b/h	x_r/h	x_t/h	x_c/h	x_b/h	x_r/h
A	ϕ_{τ_b}	–	3.02	–	–	–	302.2	–	–
	ϕ_{τ_t}	3.41	3.02	–	–	341.4	302.2	–	–
B	ϕ_{τ_b}	–	3.02	3.23	2.97	–	302.2	323.4	297.3
	ϕ_{τ_t}	2.88	3.18	2.93	3.18	288.0	317.8	292.6	317.8
C	ϕ_{τ_b}	–	2.93	3.07	2.88	–	292.6	307.2	288.0
	ϕ_{τ_t}	2.84	3.18	2.88	3.07	283.6	317.8	288.0	307.2
D	ϕ_{τ_b}	–	2.67	2.75	2.63	–	267.2	275.1	263.3
	ϕ_{τ_t}	2.33	2.88	2.88	2.84	233.3	288.0	288.0	283.6

Fig. 16 shows the variation of the Nusselt number in the cross-flow direction on the bottom wall for all cases and Prandtl numbers. In case A, a nearly symmetric variation is observed for *Nu* at both Prandtl numbers. In the corner of the wire, low values of *Nu* are observed, increasing towards the center of the channel. At $Pr = 1$, the rate of increase of *Nu* is very sharp and occurs within two wire diameters while at $Pr = 10^{-2}$ the rate of increase is lower and it occurs within four wire diameters. Towards the central part of the channel *Nu* attains a nearly constant value. The maximum value of *Nu* is higher at the higher value of Prandtl number, signifying that conductive/diffusive heat flux plays a more dominant role at the lower Prandtl numbers in this turbulent flow. In the cases with crossflow, low values of *Nu* are observed in the lee- and wind-ward corners of the wire for both Prandtl numbers. The value of *Nu* increases under the separated flow region and reaches a peak in the vicinity of the reattachment point. Note that such a rise in the heat transfer near the reattachment zone is a characteristic of separating/reattaching flows [3,7–11,19,22,25–27,31,73]. This peak value is about 50–60% higher compared to that in the case without crossflow. As the amount of crossflow increases, the peak of *Nu* becomes sharper and distinct. The peak value of *Nu* shows an abrupt increase in case D, in the high Prandtl number case. This can be attributed to an increase in the strength of the turbulence intensity and the increase in the effect of advection through the mean flow in case D. Within the separated flow region at $Pr = 1$, a kink is observed in the cases with crossflow, where *Nu* first increases, then decreases slightly and finally increases to the maximum value in the vicinity of reattachment point. This variation under the separated region occurs owing to the presence of the secondary recirculation bubble adjacent to the primary recirculation bubble in the corner of the wire. Such distribution of Nu on the bottom wall has also been observed in flow over a backward-facing step [12]. This variation under the separated flow region is not observed at the lower Prandtl number. The variation of *Nu* is monotonic under the separated flow region until it reaches a peak in the vicinity of reattachment. After reaching the peak, *Nu* shows an approximately linear decrease followed by a rapid decrease to a very small value in the lee-ward side of the wire. As mentioned in earlier studies of heat transfer in separated/reattaching flow [3,9,13–15,25,30,35,74], such a rise in the value of *Nu* can be attributed to impingement of large-scale eddies on the wall in the near-reattachment region which causes an event of downwash and brings colder fluid towards the wall. The rise of *Nu* near the reattachment region occurs due to a rise in heat transfer. The kink observed under the separated region at $Pr = 1$, has a similar origin as the flow under the separated bubble is still turbulent due to the presence of large axial flow and the impingement of large scale eddies occurs near the reattachment of the secondary bubble as well. However, at the lower Prandtl number, the effect of conduction is far more important near the secondary bubble compared to turbulent mixing and thus no abrupt variation in *Nu* is observed. Previous studies showed that wall shear stress fluctuations appears to be correlated with the heat transfer in the reattachment region [3,13,15,23], which is also evident in this study (see [45] for wall shear stress fluctuation variation). In the wind-ward side, the rapid decrease in Nu is similar to the decrease observed in the study of heat transfer under the region of turbulent separation [33], and this occurs owing to lifting of the separation streamline.

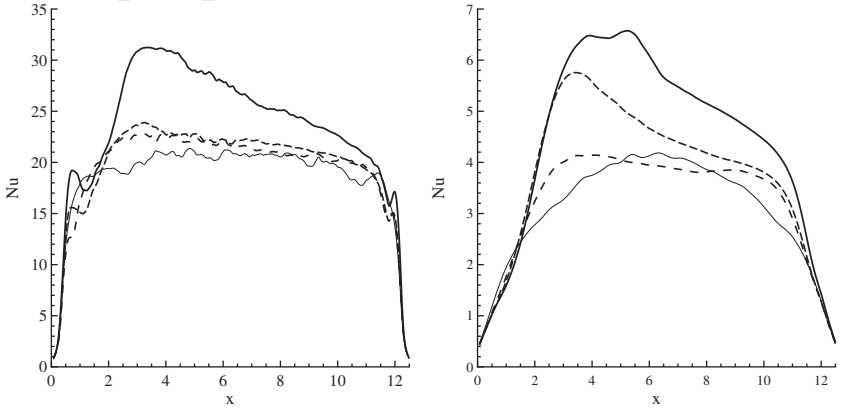

(a) $Pr = 1$ (b) $Pr = 10^{-2}$

Fig. 16. Variation of Nusselt number, *Nu*, at two Prandtl numbers, along the cross-flow direction on the bottom wall. Cases A, B, C and D are denoted by thin solid, thin dashed, thin dashed-dotted and thick solid curves, respectively.

Please cite this article in press as: R. Ranjan et al., Direct simulation of turbulent heat transfer in swept flow over a wire in a channel, Int. J. Heat Mass Transfer (2011), doi:10.1016/j.ijheatmasstransfer.2011.06.013

5.2. Temperature root-mean-square distribution

Profiles of root-mean-square, r.m.s., temperature fluctuation normalized by wall temperature heat-flux, ϕ_{rms}, at different cross-flow locations for the two Prandtl numbers are shown in Fig. 17 for all cases. Similar to wall bounded flows [61,67], peaks in ϕ_{rms} at x_c arise close to the walls for both Prandtl number cases. Obviously, there is a large change in the thickness of the thermal boundary layer with Prandtl number, the peaks are closer to the walls for $Pr = 1$ than for $Pr = 10^{-2}$. In addition, the peak ϕ_{rms} for $Pr = 1$, is an order of magnitude larger than that observed for $Pr = 10^{-2}$. This occurs because at lower Pr the stronger diffusion prevents turbulent stirring from folding the scalar field, to increase the temperature fluctuation level. The strength of the crossflow also affects the location of the peaks and the minimum of ϕ_{rms}, in particular for the low Prandtl number cases. This indicates persistence of higher levels of temperature fluctuations in the outer part of the thermal boundary layer and a slower recovery towards equilibrium levels after reattachment. At location x_b, the temperature fluctuation peak is observed near the bottom and top walls and a minimum value of ϕ_{rms} is observed towards the lower half of the channel.

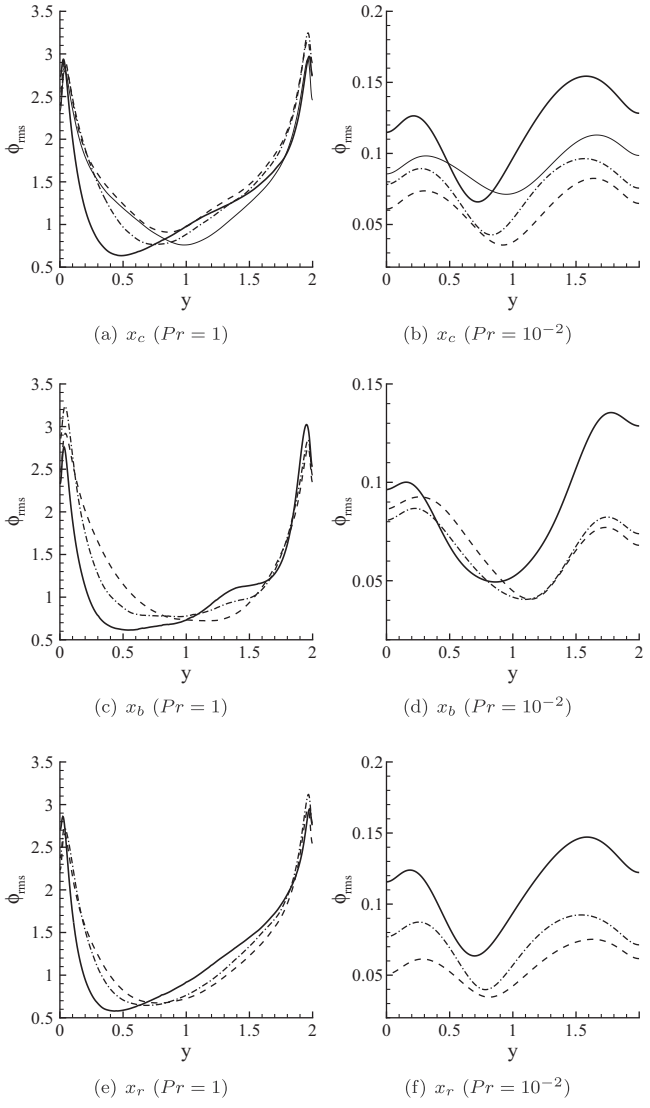

Fig. 17. R.m.s. temperature fluctuations normalized by surface temperature heat-flux at different cross-flow locations. Cases A, B, C and D are denoted by thin solid, thin dashed, thin dashed-dotted and thick solid curves, respectively.

Qualitatively, the trends for x_b and x_r are similar to those observed at x_c. Overall, the Prandtl number affects the temperature fluctuations, which is an order of magnitude higher for $Pr = 1$, and it affects the thickness of the thermal boundary layer. The crossflow introduces a shift of the location of the minimum of ϕ_{rms} towards the lower half of the channel and an increase in the magnitude of temperature fluctuations, for fixed Prandtl number, as crossflow increases. The shift of minimum occurs toward the lower wall due to an increased level of temperature fluctuations in the separated shear layer with increasing crossflow. Such a rise in the intensity of temperature fluctuation at the outer edge of the separated bubble has also been observed in flow over a two-dimensional hill [37]. After reattachment the near-wall regime recovers quickly towards equilibrium level whereas the outer part of the thermal boundary layer recovers slowly, thus even at location x_c, ϕ_{rms} shows an asymmetric variation.

5.3. Inner-scaled turbulent heat flux

The profiles of non-dimensional mean axial heat flux, defined as:

$$-\langle w'\phi'\rangle^{+} = -\frac{\langle w'T'\rangle}{\langle u_\tau\rangle\langle T_\tau\rangle}, \tag{12}$$

are investigated at different crossflow locations in Fig. 18 for all cases. In Eq. (12), $\langle u_\tau\rangle$ and $\langle T_\tau\rangle$ denote averaged values of friction velocity and surface temperature flux over all the wetted surfaces, respectively. Overall, there are two pronounced peaks close to the walls at the three locations investigated: x_c, x_b and x_r. The location of the peaks is affected by the Prandtl number, being closer to the wall for $Pr = 1$ and further away for $Pr = 10^{-2}$ due to the variation of the thermal boundary layer thickness, as noted earlier. The magnitude of the peaks is correlated with the level of temperature intensity, since the turbulent flow is unaffected by the passive scalar. As crossflow increases, a secondary peak of growing magnitude develops towards the center of the domain for $Pr = 1$ at all locations and for $Pr = 10^{-2}$ at x_b. This secondary peak is tied to the presence of the shear layer over the recirculation bubble, which entrains cold fluid towards the wall and thus, promotes mixing [13]. Note that, compared to other canonical separating/reattaching flows, in the present case the recirculation bubble is not closed in the mean sense due to presence of a net axial flow. This leads to increased velocity fluctuations in the shear layer [75], which in turn leads to enhanced mixing.

The profiles of non-dimensional mean wall-normal heat flux, defined as:

$$-\langle v'\phi'\rangle^{+} = -\frac{\langle v'T'\rangle}{\langle u_\tau\rangle\langle T_\tau\rangle}, \tag{13}$$

are investigated at different crossflow locations in Fig. 19 for all cases. At location x_c, case A shows the expected profile [61,67] which flattens towards the center of the channel, where the turbulent heat flux dominates the molecular heat flux, and near the wall $-\langle v'\phi'\rangle^{+}$ reduces sharply to zero due to the no-slip boundary condition. Furthermore, the profiles are qualitatively similar at both Prandtl numbers. However, molecular transport is dominant for $Pr = 10^{-2}$ and it penetrates deeper into the core of the channel. Note that these fluxes are an order of magnitude lower than those for the unity Prandtl number case. In the cases with crossflow, there is a strong deviation from the flattened profile in the center of the channel; the deviation increases with increasing crossflow. At location x_b, the behavior of the mean wall-normal flux for $Pr = 1$ is significantly different from that observed at other locations. Along with the peaks observed in the near-wall region, peaks are also observed above and below the center of the shear layer. Such a peak in the

Please cite this article in press as: R. Ranjan et al., Direct simulation of turbulent heat transfer in swept flow over a wire in a channel, Int. J. Heat Mass Transfer (2011), doi:10.1016/j.ijheatmasstransfer.2011.06.013

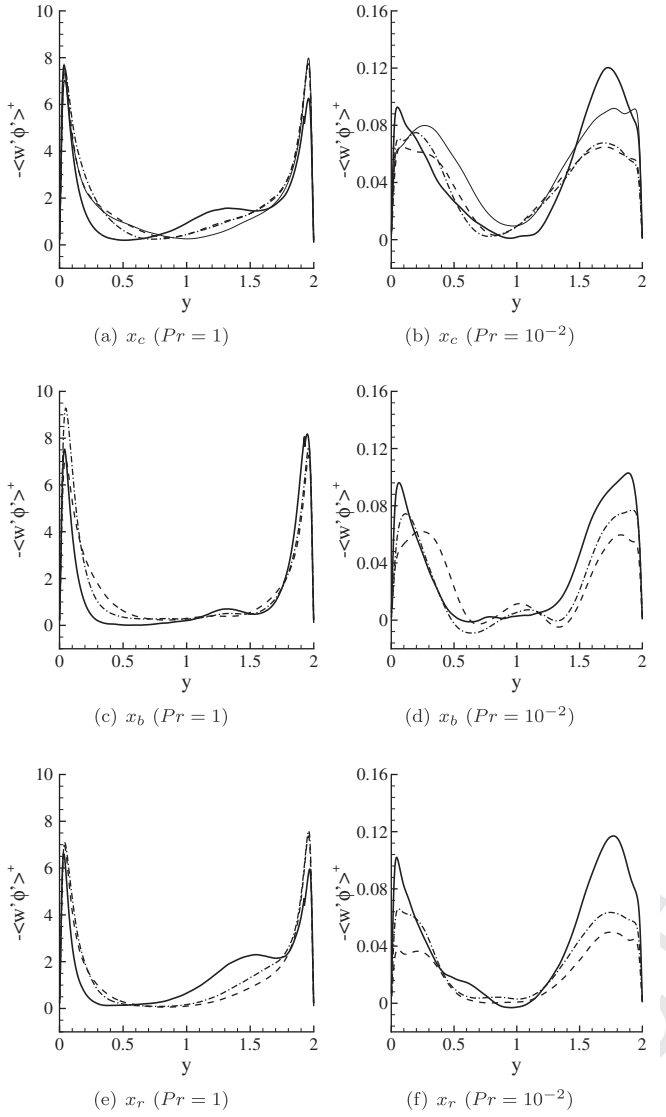

Fig. 18. Mean axial heat flux, $-\langle w'\phi' \rangle^+$, at different cross-flow locations. Cases A, B, C and D are denoted by thin solid, thin dashed, thin dashed-dotted and thick solid curves, respectively.

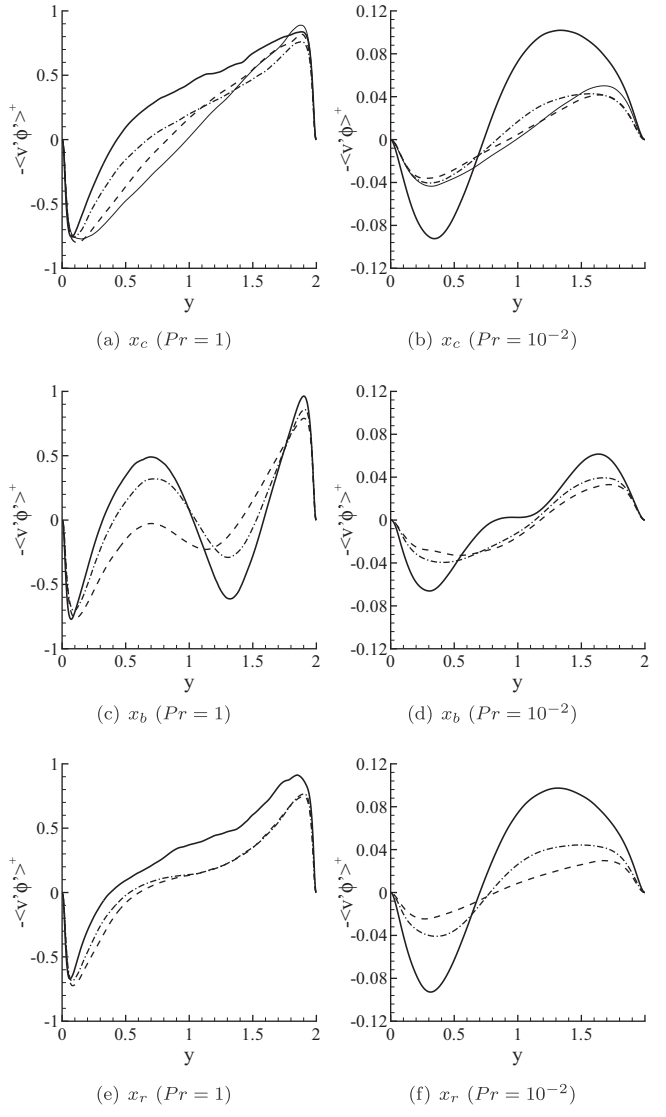

Fig. 19. Mean wall-normal heat flux, $\langle v'\phi' \rangle^+$, at different cross-flow locations. Cases A, B, C and D are denoted by thin solid, thin dashed, thin dashed-dotted and thick solid curves, respectively.

profile of wall-normal turbulent heat flux have also been observed in flow over a backward-facing step [13], which is driven by positive wall-normal velocity fluctuations [75]. However at the lower Prandtl number, no peaks are observed in the shear layer region in cases B and C, where an approximately flatten profile is observed. In case D, the behavior of the wall-normal flux is different from cases B and C which can be attributed to an increase in the level of mixing in the shear layer region due to the increased strength of the crossflow. At location x_r, the profile shows the recovery process of the flow and the temperature field approaches equilibrium, peaks start to develop in the near-wall region and flattens out towards the center of the channel. Similar to ϕ_{rms}, the outer part of the thermal boundary recovers slowly compared to the near-wall regions, as the crossflow increases. This is due to the persistence of large fluctuations in velocity and temperature fields originating in the separated shear layer.

5.4. Fluxes over the mean dividing streamline

The total heat flux through the mean dividing streamline is balanced by the heat flux occurring at the bottom wall and the volumetric sink term, obviously. The integrated mean diffusive heat flux, D_T and the integrated mean turbulent heat flux, R_T, which are given by

$$D_T = -\frac{1}{Re_z Pr}\int_{\Gamma_s} \nabla\langle\phi\rangle \cdot d\boldsymbol{l}, \tag{14}$$

and

$$R_T = \int_{\Gamma_s} \langle \boldsymbol{u}'\phi' \rangle \cdot d\boldsymbol{l}, \tag{15}$$

while the overall heat flux through the channel wall into the recirculation bubble is given by

$$Q_w = \frac{1}{Re_z Pr}\int_{\Gamma_w} \nabla\langle\phi\rangle \cdot d\boldsymbol{l} = \frac{x_r - R\sin(\gamma/2)}{Re_z Pr}, \tag{16}$$

with x_r denoting the reattachment length; see the appendix for the notation of the geometry of the recirculation bubble.

Table 4 details the values of the integrated heat flux normalized by Q_w for all cases. The resultant heat flux along with the diffusive and turbulent heat flux occurs outward from the recirculation bubble in all cases at both Prandtl numbers, except at $Pr = 1$ in case D.

Please cite this article in press as: R. Ranjan et al., Direct simulation of turbulent heat transfer in swept flow over a wire in a channel, Int. J. Heat Mass Transfer (2011), doi:10.1016/j.ijheatmasstransfer.2011.06.013

Table 4
Integrated heat fluxes over the recirculation bubble.

Case	Re_x	$Pr = 1$			$Pr = 10^{-2}$		
		$(R_T + D_T)/Q_w$	D_T/Q_w	R_T/Q_w	$(R_T + D_T)/Q_w$	D_T/Q_w	R_T/Q_w
B	417	0.25	0.02	0.23	0.32	0.30	0.02
C	842	0.11	0.01	0.10	0.23	0.21	0.02
D	1709	−0.03	0.00	−0.03	0.21	0.18	0.03

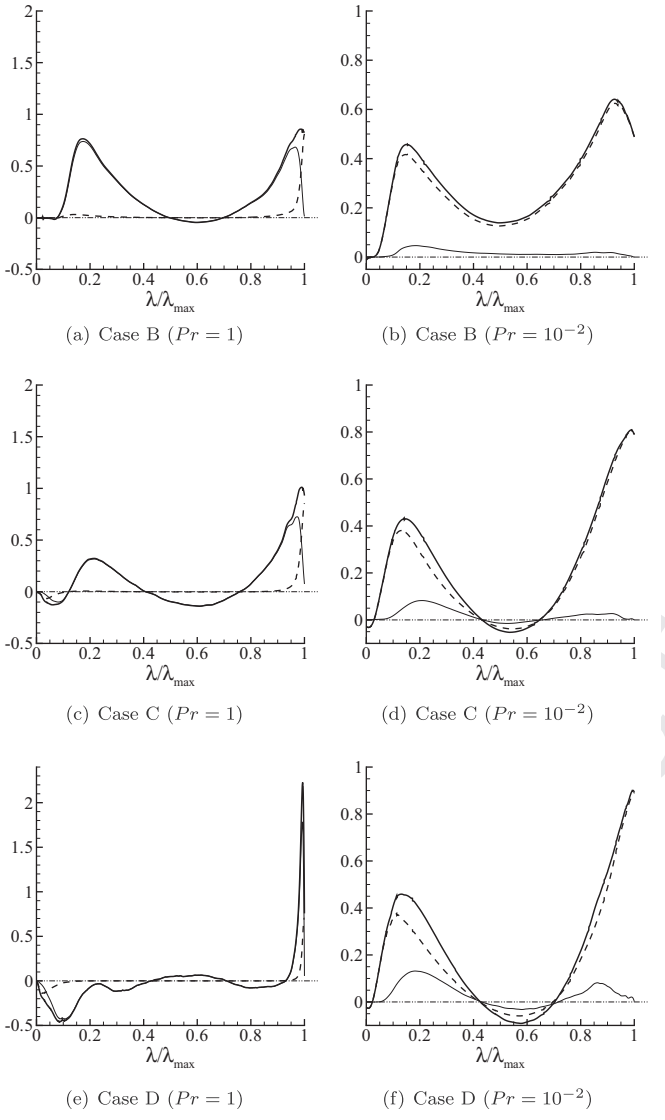

(a) Case B ($Pr = 1$) (b) Case B ($Pr = 10^{-2}$)
(c) Case C ($Pr = 1$) (d) Case C ($Pr = 10^{-2}$)
(e) Case D ($Pr = 1$) (f) Case D ($Pr = 10^{-2}$)

Fig. 20. Variation of the mean heat flux along the mean dividing streamline. Total heat flux $[\langle \boldsymbol{u}'\phi' \rangle - (Re_z Pr)^{-1} \nabla \langle \phi \rangle] \cdot \boldsymbol{n}$, diffusive heat flux $-(Re_z Pr)^{-1} \nabla \langle \phi \rangle \cdot \boldsymbol{n}$ and turbulent heat flux $\langle \boldsymbol{u}'\phi' \rangle \cdot \boldsymbol{n}$ normalized by the imposed inward heat flux $(Re_z Pr)^{-1}$, are denoted by thick solid, thin dashed and thin solid curves, respectively. The dashed-dotted curve indicates zero heat flux.

At both Prandtl numbers, increasing crossflow strength decreases the resultant heat flux outwards of the recirculation bubble. This can be attributed to the effect of increased turbulence intensity with increasing crossflow. Note that the length of the dividing streamline increases with increasing crossflow, increasing the area over which heat transfer occurs but also the volume of the recirculation bubble, enhancing the effect of the volumetric heat sink. Certainly, all these effects must balance and the resulting turbulent heat flux must satisfy energy balance. As expected, at higher Prandtl number, the turbulent heat flux across the mean dividing streamline is the dominant component of the resultant heat flux, whereas at lower Prandtl number the diffusive heat flux is the dominant component. This is consistent with the larger levels of turbulent heat fluxes observed in Section 5.3 in case of larger Prandtl number.

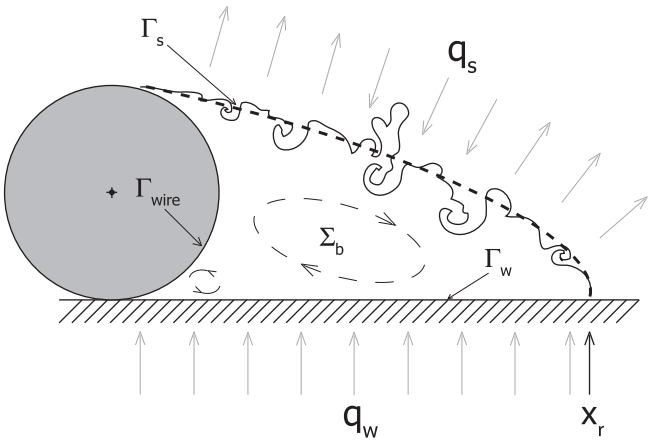

Fig. 21. Sketch of the primary and secondary recirculation bubble in the $x - y$ plane showing heat fluxes across its boundaries.

The variation of the mean pointwise heat flux components occurring through the mean dividing streamline is shown in Fig. 20. The mean dividing streamline curve is parametrized by λ and λ_{max} denotes the total length of the mean dividing streamline in the $x - y$ plane. At $Pr = 1$, the mean turbulent heat flux is larger than the mean diffusive heat flux in all cases. Near the beginning of the recirculation bubble the total heat flux, q_s, is inward and the magnitude increases with increasing crossflow. This occurs owing to a relatively lower temperature near the wire top, compared to the region above the recirculation bubble, which promotes turbulent mixing. The lower temperature is also compounded by the imposed adiabatic condition on the wire surface. Away from the wire, in cases B and C, q_s is outward, reverses towards the middle of the recirculation bubble and then turns outward again towards the second half of the recirculation bubble. Near the reattachment line, there is a sharp rise in the outward heat flux which is consistent with the rise in Nu there. Towards the center of the recirculation bubble, the variation of q_s is different in case D, it changes sign three times. There is a sharp rise in the outward mean diffusive heat flux and a sharp decrease in the mean turbulent heat flux near the reattachment zone in all cases. At $Pr = 10^{-2}$, as mentioned earlier, the role of molecular heat conduction is dominant compared to the turbulent heat flux. Higher levels of outward heat flux are observed near the top of the wire as well as near the reattachment line in all cases. With increasing crossflow, the turbulent heat flux increases near the wire top. Towards the middle of the recirculation bubble, the outward heat flux decreases. The decrease is more pronounced with increasing crossflow. This indicates that the recirculation bubble has a relatively higher temperature near the top of the wire and the reattachment regions compared to the region above it which promotes outward heat flux in these regions through molecular conduction. This further demonstrates the dominant role of the molecular conduction at lower Prandtl number, in communicating the applied heat flux at the wall towards the core of the channel, in the regions where velocity has a lower magnitude.

6. Conclusions

Results of direct numerical simulations of heat transfer in a turbulent swept flow over a wire resting on a wall of a channel are

Please cite this article in press as: R. Ranjan et al., Direct simulation of turbulent heat transfer in swept flow over a wire in a channel, Int. J. Heat Mass Transfer (2011), doi:10.1016/j.ijheatmasstransfer.2011.06.013

analyzed. The spectral element method-Fourier decomposition is used to solve the governing equations. Axial and cross-flow Reynolds numbers are 5400 and 0–1709, respectively. The present study is concerned with crossflow velocities up to 32% of the axial velocity. Temperature is modeled as a passive scalar at two Prandtl numbers, namely 1 and 10^{-2}, for four different crossflow rates.

We show, using asymptotic analysis that the temperature in the heat exchanger can be decomposed into a mean axial and planar components. The former is solved analytically in the limit of large Reynolds numbers while the latter is simulated using DNS for different levels of crossflow. Increasing crossflow, and Reynolds number, for a fixed axial flowrate increases the size of the recirculation bubble. Moreover, the presence of the wire allows for a local peak temperature region to develop along the contact line of the wire with the channel wall. In the cases at $Pr = 1$, the size of the high temperature region grows in size with increasing crossflow, whereas at $Pr = 10^{-2}$ crossflow does not have much effect due to the relative importance of diffusion over advection. This increase in the size of the high temperature region at $Pr = 1$ follows the increase in the reattachment length, which increases by about 65% from the case with the lowest to the case with the highest crossflow.

The instantaneous surface temperature shows intermittent streaks of high value embedded in low temperature regions, at $Pr = 1$ in the case without crossflow. These streaks are aligned in the axial direction. In the cases with crossflow, away from the reattachment zone, the streaky pattern of temperature is observed with streaks aligning along the net mean flow direction. Near the reattachment zone and under the primary recirculation bubble, the intermittent pattern is not evident and high temperature regions are observed. At lower Prandtl number, the streaky pattern disappears in the attached regions, as the smallest scale of temperature fluctuation increase with a decrease in Prandtl number and the temperature fluctuations does not correlate very well with the velocity fluctuations. The variation of the Nusselt number indicates higher heat transfer around reattachment which is about 50–60% higher than that observed in the case without crossflow. The maximum temperature occurs at the wire-wall contact point and it appears independent of the amount of the cross-flow and depends solely on the Prandtl number. A scaling is proposed to parametrize the maximum value of mean temperature at the corner of the wire in terms of the molecular Prandtl number.

Mean and temperature intensity as well as mean axial and normal temperature flux are investigated and their behavior in the recirculation bubbles is discussed. Inner scaled profiles of the mean temperature show deviation in the logarithmic region of the recommended formula at both Prandtl numbers. The other turbulence statistics loose symmetrical behavior as crossflow increases, implying slower recovery of thermal boundary layer after flow reattachment.

Acknowledgments

This work was supported in part by Argonne National Laboratory under subcontract 7F-01201. This research used resources of the Argonne Leadership Computing Facility at Argonne National Laboratory, which is supported by the Office of Science of the US Department of Energy under contract DE-AC02-06CH11357.

Appendix A. Temperature in the recirculation bubble

An important aspect of the present flow is to understand the behavior of the, relatively, high temperature in the recirculation zone induce by hydrodynamic confinement. Fig. 21 shows a sketch of the primary and secondary recirculation bubbles on the lee ward side of the wire. The secondary bubble is smaller and is located very close to the contact line between the wire and channel wall. In both the 'spatial' and 'periodic' arrangements discussed in the introduction, the mean crossflow section of the bubble, Σ_b, is independent of z since the mean cross-flowrate is fixed for each particular flow condition. The bubble location and size is determined only by the flow, independent of temperature. In other terms, there is no distinction between the 'spatial' and 'periodic' arrangements for the flow, the distinction is only meaningful for the temperature. The arc and segments corresponding to the wire and channel wall in contact with the recirculation bubble shown in Fig. 21 are denoted by Γ_{wire} and Γ_w, respectively. The curve defined by the mean dividing streamline is denoted by Γ_s. The constant heat flux, q_w, is applied over Γ_w while there is zero heat flux over Γ_{wire} and there is a yet unknown heat flux through Γ_s denoted by q_s. Note that the direction of the arrows indicates a qualitative direction of the total heat flux through the mean dividing streamline, it varies in the different cases studied here, and it is discussed in detail in Section 5.4. The variation of turbulent and diffusive heat fluxes across the mean dividing streamline is related to the mixing of fluid across the separating shear layer [13].

The dimensional, T, and non-dimensional, ϕ, temperatures in the 'spatial' configuration are related by Eq. (7). We will assume that ϕ approaches zero faraway upstream of the heat exchanger. The governing equation for the non-dimensional temperature is:

$$\frac{\partial\phi}{\partial t} + \nabla\cdot(\boldsymbol{u}\phi) = \frac{1}{Re_z Pr}\nabla^2\phi, \tag{17}$$

where $\boldsymbol{u} \equiv (u, v, w)$ represents the velocity field and the boundary condition $\nabla\phi\cdot\boldsymbol{n} = \epsilon$ and 0, on the channel walls and wire surface, respectively, are used. The ratio $\epsilon = h/L$ is generally a small quantity ($\epsilon \ll 1$), but its overall effect accumulates over the axial direction from $z = 0$ to $L/h = \epsilon^{-1}$ (note that all quantities are dimensionless at this stage but the original lengthscales L and h have dimensions).

It is not straightforward to determine the peak temperature at the wire-channel contact line or within the recirculation bubble but it is possible to decouple the problem into a purely axial part and a purely cross-sectional part by exploiting the fact that $\epsilon \ll 1$ and that the Reynolds number, $Re_z \gg 1$. A result of the analysis, which is common to other slender turbulent flow analysis [76], is to start by considering:

$$\phi = \epsilon[\phi_1(z) + \phi^*(x, y, z, t)] + \epsilon^2\phi_2(x, y, z, t) + \mathcal{O}(\epsilon^3). \tag{18}$$

The full solution is decomposed into a mean component that depends only on z, $\phi_1(z)$, a cross-sectional component of the same order depending x, y and z but with zero mean, and higher order terms, ϕ_2. Introducing this expansion into Eq. (17) and arranging it in the following particular manner, results in:

$$\frac{d\phi_1}{dz} = \frac{1}{Re_z Pr}\frac{d^2\phi_1}{dz^2} + q, \tag{19}$$

$$\frac{\partial\phi^*}{\partial t} + \nabla\cdot(\boldsymbol{u}\phi^*) = \frac{1}{Re_z Pr}\nabla^2\phi^* - q, \tag{20}$$

$$\frac{\partial\phi_2}{\partial t} + \nabla\cdot(\boldsymbol{u}\phi_2) = \frac{1}{Re_z Pr}\nabla^2\phi_2 - \frac{(w-1)}{\epsilon}\frac{d\phi_1}{dz}, \tag{21}$$

with boundary condition $\nabla\phi^*\cdot\boldsymbol{n} = 1$ on the channel surface and zero normal gradient over the wire for ϕ^* and zero everywhere for ϕ_2. Note that adding the three equations after multiplication by the appropriate power of ϵ results in the original equation, Eq. (17), and boundary conditions. The coefficient of the left-hand side term, affecting the first derivative of ϕ_1 with respect to z, in Eq. (19) is a consequence of the normalization chosen, since the average non-dimensional axial velocity in the channel is one. One may wonder why this term is retained in the left-hand side of Eq. (19) and why it was not dropped all together. The reason is that the solution

to such a differential equation can not be made uniformly valid over the domain of integration, $0 \leqslant z \leqslant \epsilon^{-1}$, and therefore one is forced to retain this term in the equation. The scalar constant q is introduced to ensure that the statistical steady state solution of ϕ^* is realizable. Its determination is explained below. Finally, the segregation of the equations in the form shown above is only meaningful if the last term in Eq. (21) is of order one or less. Otherwise the series expansion in Eq. (18) becomes disordered. We will show also below that in the large Reynolds number limit, our case, this term is at least of order one or even smaller.

The value of q is determined by requiring that the temperature field ϕ^* that is obtained from Eq. (20) has a statistically steady solution with zero mean and remains 'periodic' in the z direction. Obviously, this can not be accomplished without a sink term if we require, simultaneously, that mean statistics are stationary because the constant influx through the boundary must result in an increase in the temperature with time. The only way to achieve a statistically stationary state for the temperature in this 'periodic' configuration is to have a sink in Eq. (20). The magnitude of the sink can be calculated by ensemble averaging this equation and integrating over the cross sectional plane, Σ, using control volume analysis. In the stationary state, the mean scalar transport equation, obtained by ensemble averaging Eq. (20), reduces to:

$$\nabla \cdot (\langle \boldsymbol{u} \rangle \langle \phi^* \rangle + \langle \boldsymbol{u}' \phi^{*\prime} \rangle) = \frac{1}{Re_z Pr} \nabla^2 \langle \phi^* \rangle - q, \tag{22}$$

where primes denote fluctuations with respect to the ensemble averages. The derivative operators for this equation only have components on the $x - y$ plane, axial terms are zero by periodicity. The integral of Eq. (22) over Σ reduces to:

$$\int_\Sigma \nabla \cdot (\langle \boldsymbol{u} \rangle \langle \phi^* \rangle + \langle \boldsymbol{u}' \phi^{*\prime} \rangle) dxdy = \frac{1}{Re_z Pr} \int_\Sigma \nabla^2 \langle \phi^* \rangle dxdy - qS. \tag{23}$$

Using the divergence theorem and the boundary conditions $\boldsymbol{u} = 0$ at walls and the heat flux condition at the channel walls $\nabla \phi^* \cdot \boldsymbol{n} = 1$, we obtain:

$$0 = \frac{1}{Re_z Pr} \frac{(2L_x - 2R\sin(\gamma/2))}{h} - qS, \tag{24}$$

where $S \approx (2h\, L_x - \pi R^2)/h^2$ (a small correction originating in the finite contact angle of the wire is neglected). Note that all length-scales are expressed using dimensional quantities, which are therefore normalized by h. In the simulations presented in the paper, the calculation of the sink is carried out exactly, accounting for all the details of the geometry, but here we will simplify Eq. (24) by observing that $\gamma \ll 1$. Therefore, the resulting sink is given by

$$q = \frac{1}{Re_z Pr} \left(\frac{2hL_x}{2hL_x - \pi R^2} \right) \approx \frac{1}{Re_z Pr}, \tag{25}$$

where the last approximation is obtained by neglecting the area of the wire with respect to the cross section of the channel (which is appropriate in the present simulations).

Eq. (19) can now be written with the source term explicitly obtained above, resulting in

$$\frac{d^2\phi_1}{dz^2} - \alpha \frac{d\phi_1}{dz} + 1 = 0, \tag{26}$$

where

$$\alpha = Re_z Pr. \tag{27}$$

The domain of integration spans $z = 0$ to $z = \epsilon^{-1}$. The boundary conditions require matching ϕ_1 and its derivative at these two points with the solution of:

$$\frac{d^2\phi_1}{dz^2} - \alpha \frac{d\phi_1}{dz} = 0, \tag{28}$$

on $z \leqslant 0$ and $\epsilon^{-1} \leqslant z$, respectively, enforcing that both solutions are bounded at infinity. The general solution of Eq. (26) is given by

$$\phi_1 = ae^{\alpha z} + \frac{z}{\alpha} + b, \tag{29}$$

where a and b are constants. These constants can be obtained by applying the boundary conditions $\phi_1 \to 0$ as $z \to -\infty$ and matching to the two solutions (left and right) of Eq. (28), giving the final solution:

$$\phi_1 = \frac{1}{\alpha} \left(z + \frac{1 - e^{-\alpha(1/\epsilon - z)}}{\alpha} \right). \tag{30}$$

The general features of this solution are as follows: ϕ_1 is not zero at $z = 0$, due to leakage of temperature to the unheated size $z < 0$ through conduction while the temperature achieves its maximum value at $z = \epsilon^{-1}$. Note also that for large $\alpha (\gg \epsilon^{-1})$ the solution approaches $\phi_1 = z/\alpha$, which is the expected result where the temperature grows linearly with z.

Finally, we can evaluate the last term in Eq. (21). Since w obeys the no-slip boundary condition (is zero at the walls and surface of the wire) $(w - 1)$ is a quantity of order unity. Therefore:

$$\frac{(w-1)}{\epsilon} \frac{d\phi_1}{dz} = \frac{(w-1)}{\alpha\epsilon} (1 - e^{-\alpha(1/\epsilon - z)}) \sim \frac{1}{\alpha\epsilon}, \tag{31}$$

and the term is small provided $\alpha\epsilon = Re_z Pr\epsilon \gg 1$, which we can assume it is always satisfied in our case since the Péclet number, defined by

$$Pe = Re_z Pr, \tag{32}$$

is large in the turbulent regime we consider, even at our lower Prandtl number. Furthermore, the present development is a generalization of the periodic treatment, introduced in [77]. The present analysis is also valid around the transition regions where the heat flux transitions from zero to a finite value (the ends of the heat exchanger).

In conclusion, within the regime considered here, it is justifiable to consider only the dynamics of ϕ^* since they denote the deviation with respect to the axial mean $\phi_1(z)$, which can be obtained analytically. All other spatial variations of the statistics in the cross sectional plane, $x - y$, are reproduced by the 'periodic' ϕ^*. Therefore, in the paper we have discussed the statistics of ϕ^* and for ease of notation we have dropped the superscript since we have not made reference to ϕ_1 at any other location.

References

[1] T. Ota, Survey of heat transfer in separated and reattached flows, Appl. Mech. Rev. 53 (2000) 219–235.
[2] H. Nishiyama, T. Ota, K. Sato, Temperature fluctuations in a separated and reattached turbulent flow over a blunt flat plate, Wärme-und StoffüBertragung 23 (1988) 275–281.
[3] J.C. Vogel, J.K. Eaton, Combined heat transfer and fluid dynamic measurements downstream of a backward-facing step, J. Heat Mass Transfer 107 (1985) 922–929.
[4] E.M. Sparrow, S.S. Kang, W. Chuck, Relation between the points of flow reattachment and maximum heat transfer for regions of flow separation, Int. J. Heat Mass Transfer 30 (1987) 1237–1246.
[5] T. Ota, H. Nishiyama, A correlation of maximum turbulent heat transfer coefficient in reattachment flow region, Int. J. Heat Mass Transfer 30 (1987) 1193–1200.
[6] K. Abe, T. Kondoh, Y. Nagano, A new turbulence model for predicting fluid flow and heat transfer in separating and reattaching flows – II. Thermal field calculations, Int. J. Heat Mass Transfer 38 (1995) 1467–1481.
[7] H.I. Abu-Mulaweh, T.S. Chen, B.F. Armaly, Turbulent natural convection flow over a backward-facing step, Exp. Heat Transfer 12 (1999) 295–308.
[8] R.V.R. Avancha, R.H. Pletcher, Large eddy simulation of the turbulent flow past a backward-facing step with heat transfer and property variations, Int. J. Heat Fluid Flow 23 (2002) 601–614.

Please cite this article in press as: R. Ranjan et al., Direct simulation of turbulent heat transfer in swept flow over a wire in a channel, Int. J. Heat Mass Transfer (2011), doi:10.1016/j.ijheatmasstransfer.2011.06.013

[9] K. Heyerichs, A. Pollard, Heat transfer in separated and impinging turbulent flows, Int. J. Heat Mass Transfer 39 (1996) 2385–2400.
[10] Y.T. Chen, J.H. Nie, B.F. Armaly, H.T. Hsieh, Turbulent separated convection flow adjacent to backward-facing step-effects of step height, Int. J. Heat Mass Transfer 49 (2006) 3670–3680.
[11] H. Lan, B.F. Armaly, J.A. Drallmeier, Three-dimensional simulation of turbulent forced convection in a duct with backward-facing step, Int. J. Heat Mass Transfer 52 (2009) 1690–1700.
[12] F.K. Tsou, S.-J. Chen, W. Aung, Starting flow and heat transfer downstream of a backward-facing step, J. Heat Transfer 113 (1991) 583–589.
[13] A. Keating, U. Piomelli, K. Bremhorst, S. Nešić, Large eddy simulation of heat transfer downstream of a backward-facing step, J. Turbul. 5 (2004) 1–27.
[14] G.H. Rhee, H.J. Sung, Enhancement of heat transfer in turbulent separated and reattaching flow by local forcing, Numer. Heat Transfer A 37 (2000) 733–753.
[15] O. Labbé, P. Sagaut, E. Montreuil, Large-eddy simulation of heat transfer over a backward-facing step, Numer. Heat Transfer A 42 (2002) 73–90.
[16] K. Sugawara, H. Yoshikawa, T. Ota, LES of turbulent separated flow and heat transfer in a symmetric expansion plane channel, J. Fluids Eng. 127 (2005) 865–871.
[17] V.I. Terekhov, N.I. Yarigina, R.F. Zhdanov, Heat transfer in turbulent separated flows in the presence of high free-stream turbulence, Int. J. Heat Mass Transfer 46 (2003) 4535–4551.
[18] E. Abu-Nada, A. Al-Sarkhi, B. Akash, I. Al-Hinti, Heat transfer and fluid flow characteristics of separated flows encountered in a backward-facing step under the effect of suction and blowing, J. Heat Transfer 129 (2007) 1517–1528.
[19] A. Kitoh, K. Sugawara, H. Yoshikawa, T. Ota, Expansion ratio effects on three-dimensional separated flow and heat transfer around backward-facing steps, J. Heat Transfer 129 (2007) 1141–1155.
[20] H. Abu-Mulaweh, Investigations on the effect of backward-facing and forward-facing steps on turbulent mixed-convection flow over a flat plate, Exp. Heat Transfer 22 (2009) 117–127.
[21] S.A.G. Nassab, R. Moosavi, S.M.H. Sarvari, Turbulent forced convection flow adjacent to inclined forward step in a duct, Int. J. Therm. Sci. 48 (2009) 1319–1326.
[22] K. Hourigan, L.W. Welch, M.C. Thompson, P.I. Cooper, M.C. Welsh, Augmented forced convection heat transfer in separated flow around a blunt flat plate, Exp. Therm. Fluid Sci. 4 (1991) 182–191.
[23] D. Tafti, Vorticity dynamics and scalar transport in separated and reattached flow on a blunt plate, Phys. Fluids A 5 (1993) 1661–1673.
[24] G.H. Rhee, H.J. Sung, A nonlinear low-Reynolds-number k–ϵ model for turbulent separated and reattaching flows – ii. Thermal field computations, Int. J. Heat Mass Transfer 39 (1996) 3465–3474.
[25] P. Marty, F. Michel, P. Tochon, Experimental and numerical study of heat transfer along a blunt flat plate, Int. J. Heat Mass Transfer 51 (2008) 13–23.
[26] Y. Nagano, H. Hattori, T. Houra, DNS of velocity and thermal fields in turbulent channel flow with transverse-rib roughness, Int. J. Heat Fluid Flow 25 (2004) 393–403.
[27] T.-M. Liou, J.-J. Hwang, S.-H. Chen, Simulation and measurement of enhanced turbulent heat transfer in a channel with periodic ribs on one principal wall, Int. J. Heat Mass Transfer 36 (1993) 507–517.
[28] A. Tariq, K. Singh, P. Panigrahi, Flow and heat transfer in a rectangular duct with single rib and two ribs mounted on the bottom surface, J. Enhanc. Heat Transfer 10 (2003) 171–198.
[29] K.J. Hsieh, F.S. Lien, Conjugate turbulent forced convection in a channel with an array of ribs, Int. J. Numer. Methods Heat Fluid Flow 15 (2005) 462–482.
[30] S. Acharya, S. Dutta, T.A. Myrum, Heat transfer in turbulent flow past a surface-mounted two-dimensional rib, J. Heat Transfer 120 (1998) 724–734.
[31] G. Rau, M. Cakan, D. Moeller, T. Arts, The effect of periodic ribs on the local aerodynamic and heat transfer performance of a straight cooling channel, J. Turbomach. 120 (1998) 368–375.
[32] J.C. Han, J.S. Park, Developing heat transfer in rectangular channels with rib turbulators, Int. J. Heat Mass Transfer 31 (1988) 183–195.
[33] R.B. Rivir, J.P. Johnston, J.K. Eaton, Heat transfer on a flat surface under a region of turbulent separation, J. Turbomach. 116 (1994) 57–62.
[34] P.R. Spalart, M.K. Strelets, Mechanisms of transition and heat transfer in a separation bubble, J. Fluid Mech. 403 (2000) 329–349.
[35] H.S. Choi, K. Suzuki, Large eddy simulation of turbulent flow and heat transfer in a channel with one wavy wall, Int. J. Heat Fluid Flow 26 (2005) 681–694.
[36] M.V. Pham, F. Plourde, S.K. Doan, Turbulent heat and mass transfer in sinusoidal wavy channels, Int. J. Heat Fluid Flow 29 (2008) 1240–1257.
[37] T. Houra, Y. Nagano, Turbulent heat and fluid flow over a two-dimensional hill, Flow Turbul. Combust. 83 (2009) 389–406.
[38] J. Medwell, W. Morris, J. Xia, C. Taylor, An investigation of convective heat transfer in a rotating coolant channel, J. Turbomach. 113 (1991) 354–359.
[39] D. Ryu, D. Choi, V. Patel, Analysis of turbulent flow in channels roughened by two-dimensional ribs and three-dimensional blocks: part II: heat transfer, Int. J. Heat Fluid Flow 28 (2007) 1112–1124.
[40] K. Takase, Experimental and analytical studies on turbulent heat transfer performance of a fuel rod with spacer ribs for high temperature gas-cooled reactors, Nucl. Eng. Des. 154 (1995) 345–356.
[41] Y. Suh, M. Lightstone, Numerical simulation of turbulent flow and mixing in a rod bundle geometry, Nucl. Energ. J. Br. Nucl. Energ. Soc. 43 (2004) 153–163.
[42] J. Gou, Z. Shang, Y. Ishiwarari, Y. Oka, M. Yamakawa, S. Ikejiri, CFD analysis of heat transfer in subchannels of a super fast reactor, Nucl. Eng. Des. 240 (2010) 1819–1829.
[43] W. Kim, S. He, J. Jackson, Assessment by comparison with DNS data of turbulence models used in simulations of mixed convection, Int. J. Heat Mass Transfer 51 (2008) 1293–1312.
[44] P. Fischer, J. Lottes, A. Siegel, G. Palmiotti, Large eddy simulation of wire-wrapped fuel pins I: hydrodynamics in a periodic array, in: Joint International Topical Meeting on Mathematics and Computation and Supercomputing in Nuclear Applications, Monterey, CA, pp. 1–7.
[45] R. Ranjan, C. Pantano, P. Fischer, Direct simulation of turbulent swept flow over a wire in a channel, J. Fluid Mech. 651 (2010) 165–209.
[46] J. Hébrard, O. Métais, M. Salinas-Vasquez, Large-eddy simulation of turbulent duct flow: heating and curvature effects, Int. J. Heat Fluid Flow 25 (2004) 569–580.
[47] R. Mathews, C. Balaji, T. Sundararajan, Computation of conjugate heat transfer in the turbulent mixed convection regime in a vertical channel with multiple heat sources, Heat Mass Transfer 43 (2007) 1063–1074.
[48] W. Raza, K.-Y. Kim, Comparative analysis of flow and convective heat transfer between 7-pin and 19-pin wire-wrapped fuel assemblies, J. Nucl. Sci. Technol. 45 (2008) 653–661.
[49] K. Horiuti, Assessment of two-equation models of turbulent passive-scalar diffusion in channel flow, J. Fluid Mech. 238 (1992) 405–433.
[50] N. Kasagi, A. Kuroda, M. Hirata, Numerical investigation of near-wall turbulent heat transfer taking into account the unsteady heat conduction in the solid wall, J. Heat Transfer 111 (1989) 385–392.
[51] I. Tiselj, R. Bergant, B. Mavko, I. Bajsić, G. Hetsroni, Dns of turbulent heat transfer in channel flow with heat conduction in the solid wall, J. Heat Transfer 123 (2001) 849–857.
[52] J. Jeong, F. Hussain, On the identification of a vortex, J. Fluid Mech. 285 (1995) 69–94.
[53] S. Song, J.K. Eaton, Flow structures of a separating, reattaching, and recovering boundary layer for a large range of Reynolds number, Exp. Fluids 36 (2004) 642–653.
[54] H. Le, P. Moin, J. Kim, Direct numerical simulation of turbulent flow over a backward-facing step, J. Fluid Mech. 330 (1997) 349–374.
[55] I. Lee, H.J. Sung, Multiple-arrayed pressure measurement for investigation of the unsteady flow structure of a reattaching shear layer, J. Fluid Mech. 463 (2002) 377–402.
[56] H.-J. Kaltenbach, G. Janke, Direct numerical simulation of flow separation behind a swept, rearward-facing step at $Re_H = 3000$, Phys. Fluids 12 (2000) 2320.
[57] T.W.H. Sheu, H.P. Rani, Exploration of vortex dynamics for transitional flows in a three-dimensional backward-facing step channel, J. Fluid Mech. 550 (2006) 61–83.
[58] R.D. Henderson, Unstructured Spectral Element Methods: Parallel Algorithms and Simulations, Ph.D. Thesis, Princeton University, 1994.
[59] R.D. Henderson, G.E. Karniadakis, Unstructured spectral element methods for simulation of turbulent flows, J. Comp. Phys. 122 (1995) 191–217.
[60] H. Tennekes, J.L. Lumley, A First Course in Turbulence, MIT Press, 1972.
[61] J. Kim, P. Moin, Transport of passive scalars in a turbulent channel flow, in: Turbulent Shear Flows, vol. 6, 1989, pp. 85–96. Q1
[62] H. Kawamura, H. Abe, Y. Matsuo, DNS of turbulent heat transfer in channel flow with respect to Reynolds and Prandtl number effects, Int. J. Heat Fluid Flow 20 (1999) 196–207.
[63] N. Kasagi, Y. Tomita, A. Kuroda, Direct numerical simulation of passive scalar field in a turbulent channel flow, J. Heat Transfer 114 (1992) 598–606.
[64] Y. Iritani, N. Kasagi, M. Hirata, Heat transfer mechanism and associated turbulence structure in the near-wall region of a turbulent boundary layer, in: Symposium on Turbulent Shear Flows, Karlsruhe, Germany, vol. 4, 1983, pp. 17.31–17.36.
[65] B. Debusschere, C.J. Rutland, Turbulent scalar transport mechanisms in plane channel and couette flows, Int. J. Heat Mass Transfer 47 (2004) 1771–1781.
[66] P.R. Spalart, G.N. Coleman, Numerical study of a separation bubble with heat transfer, Eur. J. Mech. B. Fluids 16 (1997) 169–189.
[67] H. Kawamura, K. Ohsaka, H. Abe, K. Yamamoto, DNS of turbulent heat transfer in channel flow with low to medium-high Prandtl number fluid, Int. J. Heat Fluid Flow 19 (1998) 482–491.
[68] F. Schwertfirm, M. Manhart, DNS of passive scalar transport in turbulent channel flow at high schmidt numbers, Int. J. Heat Fluid Flow 28 (2007) 1204–1214.
[69] R.A. Antonia, J. Kim, Turbulent Prandtl number in the near-wall region of a trubulent channel flow, Int. J. Heat Mass Transfer 34 (1991) 1905–1908.
[70] H.G. Nepomuceno, M. Lueptow, Pressure and shear stress measurements at the wall in a turbulent boundary layer on a cylinder, Phys. Fluids 9 (1997) 2732.
[71] B.A. Kader, Temperature and concentration profiles in fully turbulent boundary layers, Int. J. Heat Mass Transfer 24 (1981) 1541–1544.
[72] Y. Na, T.J. Hanratty, Limiting behavior of turbulent scalar transport close to a wall, Int. J. Heat Mass Transfer 43 (2000) 1749–1758.
[73] H. Abu-Mulaweh, Turbulent natural-convection flow over a vertical forward-facing step, Exp. Heat Transfer 15 (2002) 49–69.
[74] D.B. Spalding, Heat transfer from turbulent separated flows, J. Fluid Mech. 27 (1967) 97–109.
[75] M.M. Rogers, R.D. Moser, Direct simulation of a self-similar turbulent mixing layer, Phys. Fluids 6 (1994) 903–923.
[76] F. Higuera, J. Jimenez, A. Linan, Asymptotic solution of the turbulent mixing layer for velocity ratio close to unity, in: Proceedings of the Summer Program, Center for Turbulence Research, 1996, pp. 207–215. Q2
[77] S. Patankar, C. Liu, E. Sparrow, Fully developed flow and heat transfer in ducts having streamwise-periodic variations of cross-sectional area, J. Heat Transfer 99 (1977) 180–186.

Please cite this article in press as: R. Ranjan et al., Direct simulation of turbulent heat transfer in swept flow over a wire in a channel, Int. J. Heat Mass Transfer (2011), doi:10.1016/j.ijheatmasstransfer.2011.06.013